


Examining the Developmental Trajectory of an *in Vitro* Model of Mouse Primordial Germ Cells following Exposure to Environmentally Relevant Bisphenol A Levels

Steen K.T. Ooi,¹ Hui Jiang,¹ Yanyuan Kang,¹ and Patrick Allard^{1,2} 

¹UCLA Institute for Society & Genetics, University of California, Los Angeles, Los Angeles, California, USA

²Molecular Biology Institute, University of California, Los Angeles, Los Angeles, California, USA

BACKGROUND: Animal-based studies indicate that bisphenol A (BPA) exposure is detrimental to reproductive health, but its impact on the earliest stages of germ cell development remains poorly defined.

OBJECTIVES: Using a murine *in vitro* model of early germ cell specification and differentiation, we sought to assess whether exposure to low levels of BPA prior to formation of primordial germ cells (PGCs) alters their differentiation trajectory and unique molecular program.

METHODS: We used an established method of *in vitro* differentiation of mouse embryonic stem cells (ESCs) into epiblast-like cells (EpiLCs) followed by PGC-like cells (PGCLCs), which together recapitulate defined stages of early germ cell development. Cellular consequences were determined using hemocytometer-based cell counting, fixation, and intracellular staining, followed by flow cytometry/fluorescence-activated cell sorting (FACS) of cells exposed to increasing concentrations (range: 1 nM–10 μ M) of BPA. To interrogate and characterize gene expression differences resulting from BPA exposure, we also generated RNA-seq libraries from RNA extracted from FACS-purified PGCLCs and performed transcriptome analysis using bioinformatics-based approaches.

RESULTS: Exposure of EpiLCs to BPA resulted in higher numbers of cells that were associated with a higher proportion of cells in S-phase as well as a lower proportion undergoing apoptosis; this difference occurred in a concentration-dependent manner. Exposure also resulted in a greater fraction of EpiLCs showing signs of DNA damage. Remarkably, EpiLC exposure did not negatively affect PGC specification and resulted in a concentration-dependent effect on PGCLC proliferation in XX but not XY cells. PGCLC transcriptome analysis revealed an aberrant program with significant deregulation of X-linked genes and retrotransposon expression. Differential gene expression analysis also revealed the deregulation of genes associated with lipid metabolism as well as deregulated expression of genes associated with later stages of gametogenesis.

CONCLUSIONS: To the best of our knowledge our findings represent the first characterization of the consequences of early BPA exposure on a model of mammalian PGC development, highlighting altered cell behavior, altered underlying pathways, and altered molecular processes. <https://doi.org/10.1289/EHP8196>

Introduction

Germ cells represent the bridge between generations, essential for the formation of new individuals in sexually reproducing organisms. It is therefore crucial that the information they contain is both correctly established, maintained, and executed over the course of development. Errors in these crucial developmental steps manifest as developmental defects, disease, and an overall reduction in reproductive fitness (Larose 2019).

In mammals, gametes are specified initially as primordial germ cells (PGCs), which in mice arise in embryonic day 6.5 (E6.5) postimplantation embryos, from cells derived in the epiblast layer (Gardner and Rossant 1979; Snow 1981). Over the course of their development, PGCs undergo a unique and complex reprogramming in both transcriptional and epigenetic signatures, necessary for the correct formation of germ cells and resulting gametes in the adult animal. Errors in reprogramming and proper germ cell function lie at the root of a number of adverse health outcomes, including chromosome anomalies, birth defects (Hassold et al. 1993; Hassold and Hunt 2001; Hunt and Hassold 2008), infertility (Matzuk and Lamb 2008), and cancer

(Oosterhuis and Looijenga 2005). Perturbations in normal germ cell development are therefore something that must be minimized or, ideally, altogether avoided.

Germ cells at late stages of their development are extremely sensitive to environmental exposures, as highlighted by the breadth of chemicals exhibiting germ cell toxicity in both humans and rodents. These environmental agents include compounds as diverse as components of plastics (Hunt et al. 2003), pesticides (Harkonen 2005), cigarette smoke (Mailhes et al. 2000), anti-anxiety medication (Tanrikut et al. 2010), chemotherapeutic agents (Hales et al. 2005), and many more (Pacchierotti and Ranaldi 2006). However, there is a remarkable paucity of information concerning the impact of environmental agents on the earlier stages of germ cell development described above. Existing studies on the impact of toxicants on the window of germ cell development when they are potentially most vulnerable (i.e., when PGCs are present) are obfuscated by the difficulties intrinsic to their study: PGCs exist for a short developmental window between E6.5 and E11.5 in the developing embryo (Ginsburg 1990; Molyneaux 2001), and toxicant exposure typically covers multiple stages of germ cell development and differentiation; consequences of exposure can only be analyzed well after PGCs have differentiated into later developmental stages (e.g., mature oocytes or spermatozoa) or in resultant offspring derived from such gametes (reviewed in Matuszczak 2019).

In this context, the development of *in vitro* methods to differentiate embryonic stem cells (ESCs) into PGC-like cells (PGCLCs), such as those pioneered by Saitou et al., provide an invaluable system to study environmental impacts on early germ cells (Hayashi et al. 2011). Transcriptome and methylome analyses indicate that PGCLCs closely mirror the expression program and epigenetic reprogramming observed in *in vivo* PGCs and have the ability to give rise to live offspring (Hayashi et al. 2011; Shirane et al. 2016), indicating the recapitulation of all essential steps for gamete generation. Furthermore, because differentiation is ordered and controlled by the provision of specified growth factors in the

Address correspondence to Patrick Allard, UCLA Institute for Society & Genetics, 621 Charles E. Young Dr. South, Life Science Building 3360, University of California, Los Angeles, Los Angeles, CA 90095 USA. Email: pallard@ucla.edu

Supplemental Material is available online (<https://doi.org/10.1289/EHP8196>).

The authors declare they have no actual or potential competing financial interests.

Received 1 September 2020; Revised 27 August 2021; Accepted 31 August 2021; Published 29 September 2021.

Note to readers with disabilities: *EHP* strives to ensure that all journal content is accessible to all readers. However, some figures and Supplemental Material published in *EHP* articles may not conform to 508 standards due to the complexity of the information being presented. If you need assistance accessing journal content, please contact ehponline@niehs.nih.gov. Our staff will work with you to assess and meet your accessibility needs within 3 working days.

culture media, the system is highly tractable, allowing spatial and temporal control of environmental exposure.

At moderate to high exposures, the plastic-manufacturing chemical bisphenol A (BPA) is a well-described reproductive toxicant in a wide variety of species, including nematodes (Allard and Colaiacovo 2010), fish (Chen et al. 2017), mouse (Hunt et al. 2003; Susiarjo et al. 2007), and humans (Briño-Enríquez et al. 2011). Studies focused on the mammalian germline indicate detrimental consequences of BPA exposure on both male and female gametogenesis (Prins et al. 2019). However, owing to the complexity of gametogenesis, the delineation of critical phases for exposure, especially at the earlier stages of germ cell development, the capture of more subtle effects resulting from exposure to low environmentally relevant BPA levels, and the potential mechanisms involved all remain poorly defined.

Here, we leveraged the stepwise generation of PGCLCs to perform developmental stage-specific exposure. Specifically, we aimed to test whether exposure to low, environmentally relevant levels of BPA prior to initiation of the PGCLC program could alter their induction and/or developmental trajectory.

Methods

PGCLC Culture System

Murine PGCLCs were derived according to the two-stage protocol [ESC to Epiblast-like cell (EpiLC) followed by induction into PGCLCs as previously described by Hayashi et al. (2011)], using ESCs carrying B lymphocyte-induced maturation protein 1 *Blimp1-mVenus* and *Stella-ECFP* reporter transgenes (hereafter referred to as BVSC cells) (Ohinata et al. 2008). Unless indicated otherwise, all experiments described herein were performed on genetically female (XX) *Blimp1-mVenus Stella-ECFP* (BVSC, clone H18) ESCs. All ESC lines used in this study, BVSC-H18, BVSC-R8, and v6.5, were obtained from M. Saitou (kind gift). All cells were cultured in a 37°C tissue culture incubator with 5% CO₂. Briefly, BVSC ESCs were seeded onto Poly-L-ornithine (0.001%; A-004-C; Sigma-Aldrich) and laminin-300 (300 ng/mL; L2020; Sigma-Aldrich) coated wells and cultured in 2i+LIF [N2B27 Media, CHIR99021 (30 μM; NC9785126; ThermoFisher Scientific), PD0325901 (10 μM; NC9753132; ThermoFisher Scientific)], ESGRO® Leukemia Inhibitory Factor (LIF) (1,000 U/mL, ESG1106; Sigma-Aldrich), 1,000 U/mL for 2 d. Typically, ESCs were cultured in either 24- or 12-well format, seeding 4 × 10⁴ or 8 × 10⁴ cells, respectively. EpiLCs were induced by seeding 4 × 10⁴ or 8 × 10⁴ cells onto human plasma fibronectin- (HPF) (16.7 μg/mL; 33016015; ThermoFisher Scientific) coated wells of either a 24- or 12-well plate, respectively, in EpiLC Media (N2B27 medium containing activin A (20 ng/mL; 50-398-465; ThermoFisher Scientific), basic fibroblast growth factor (bFGF) (12 ng/mL; 3139FB025; R&D Systems), and KnockOut Serum Replacement (KSR, 1%; ThermoFisher Scientific). For ESC and EpiLC culture, cells were cultured on GenClone® tissue culture plates (tissue culture-treated polystyrene, Genesee Scientific). After 40 h, cells were collected by incubation with TrypLE™ Select (1X) (ThermoFisher Scientific). PGCLC induction was initiated by seeding 3 × 10³ cells in a well of a low-cell-binding U-bottom 96-well virgin polystyrene suspension culture plate [either Genesee Scientific or Nunclon Sphera-Treated U-shaped 96-well plates (ThermoFisher Scientific)] in GK15 Media [GMEM (ThermoFisher Scientific)] supplemented with 15% knockout serum replacement (KSR), 0.1 mM minimal essential medium nonessential amino acids (MEM-NEAA), 1 mM sodium pyruvate, 0.1 mM 2-mercaptoethanol, 100 U/mL penicillin, 0.1 mg/mL streptomycin, and 2 mM L-glutamine in the presence of the cytokines bone morphogenetic protein 4 (BMP4;

500 ng/mL; 5020-BP-010/CF; R&D Systems), leukemia inhibitory factor (LIF; 1,000 U/mL; ESG1106; Sigma-Aldrich), stem cell factor (SCF; 100 ng/mL; 50-399-595; R&D Systems), bone morphogenetic protein 8b (BMP8b; 500 ng/mL; 7540-BP-025; R&D Systems), and epidermal growth factor (EGF; 50 ng/mL; 2028EG200; R&D Systems). Cells were cultured for 5 d before collection and dissociation using TrypLE™ Select for further analysis.

Differentiation Model and Exposure Paradigm

ES cells were maintained on 2i+LIF conditioned media for 2–3 d before being induced into EpiLCs by switching to EpiLC media (Figures 1A and 2A). Because the transition from ESCs to EpiLCs itself involves profound molecular reprogramming in DNA methylation (reviewed in Wu and Zhang 2014), exposures were performed after that first reprogramming phase during a 24-h window prior to PGCLC induction and washed out when cells were switched to PGCLC culture medium. Because even low quantities of dimethylsulfoxide (DMSO) can alter ESC differentiation (Adler et al. 2006) and BPA is soluble in water at the concentration range tested (Shareef et al. 2006; Plahuta et al. 2015), BPA (239658; Sigma-Aldrich) was dissolved in autoclaved, double-distilled water (ddH₂O) at 55°C for several hours at a concentration of 1 mM (equivalent to 0.228 mg/mL), before filtering and aliquoting, followed by storage at –20°C. The amount of BPA available in frozen stocks was verified by ELISA (BPA ELISA Kit; Detroit R & D, Inc.; see “BPA ELISA” section, Figure S1, and Excel Table S1). For each exposure experiment, aliquots of 1 mM BPA stocks were thawed and diluted in appropriate media (2i+LIF, EpiLC media, or PGCLC induction media). For water controls, the same volume of autoclaved ddH₂O as the highest concentration of BPA dissolved in water being used was added to the culture media. Of the 4-order magnitude range of BPA concentrations tested, the 1–100 nM range was chosen to encompass the reported human BPA environmentally relevant range detected in serum, urine, and reproductive fluids (Vandenberg 2007), whereas the 1 μM and 10 μM concentrations represent moderate exposure levels comparable to those found in rodent *in vivo* models (Allard 2014).

BPA ELISA

ELISA was performed according to the manufacturer’s protocol. Briefly, a six-point standard curve was set up, with BPA ranging in concentration between 1 × 10⁶ pg/mL and 1 × 10¹ pg/mL, generated by 10-fold serial dilution using kit-provided BPA or dissolved BPA stock and sample dilution buffer. Samples were mixed with an equal volume (100 μL) of diluted BPA-HRP conjugate and incubated at room temperature for 2 h. Plates were then washed three times in 400 μL 1 × wash buffer before incubation with 200 μL TMB substrate at room temperature for 30 min. Development was stopped by addition of 50 μL of 2N sulfuric acid, and absorbance at 450 nm was read on a Tecan Infinite® M1000 plate reader (Tecan). Corrected absorbance readings were then used to generate standard curves, according to the manufacturer’s instructions.

Cell Proliferation Analysis

Cells were exposed to a range of BPA concentrations: 10 nM, 100 nM, 1 μM and 10 μM. For ESCs, cells were exposed for 48 h; for EpiLCs, cells were exposed for 24 h. Proliferation was assessed using several methods: numbers of viable cells were determined by Trypan blue (0.4%, 3–5 min incubation) exclusion using a Countess II FL Automated Cell Counter (ThermoFisher Scientific); by dual staining with anti-BrdU antibody (see

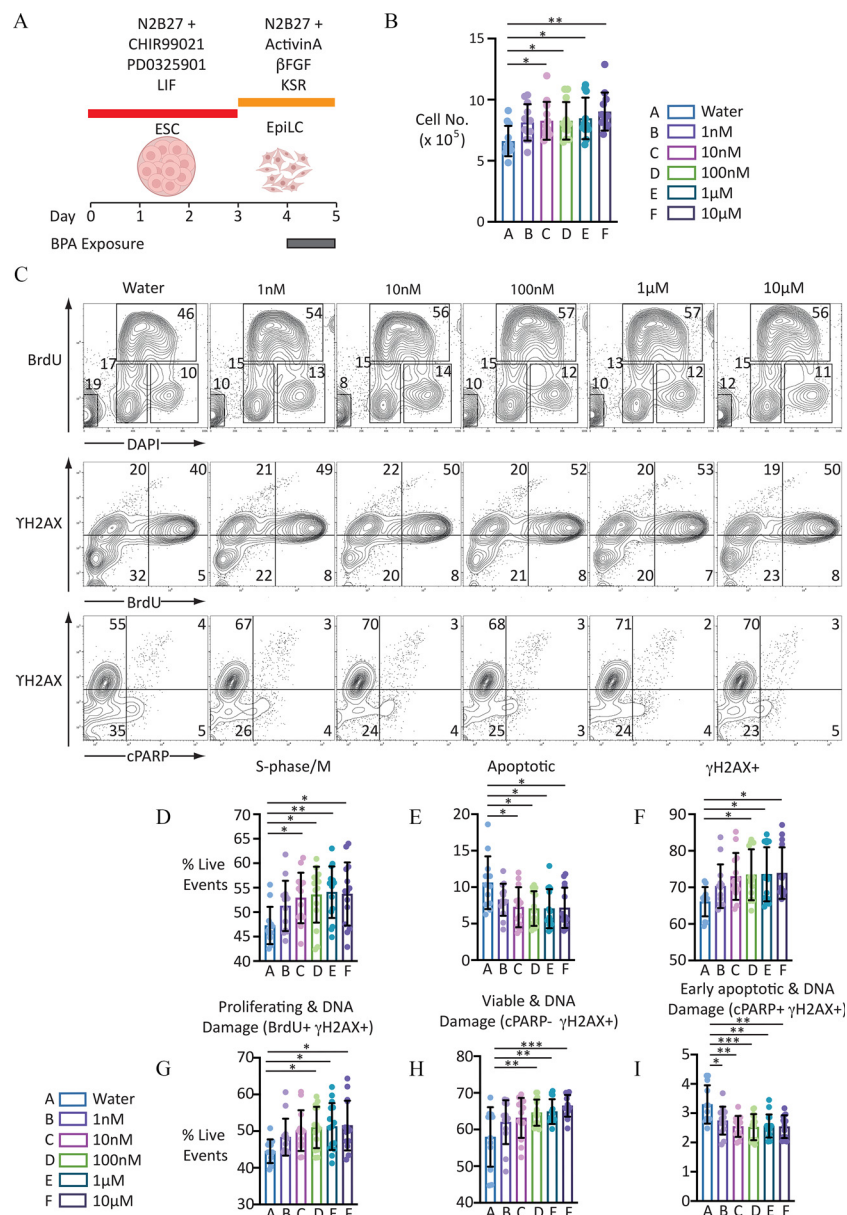


Figure 1. Proliferation analysis of EpiLCs to BPA for 24 h. (A) Graphic illustrating BPA exposure and cell differentiation strategy. [Illustration in part created with ©BioRender ([biorender.com](https://www.biorender.com)), per the Biorender terms and conditions.] (B) Scatter-bar plot indicating cell counts of EpiLCs exposed to the different BPA concentrations indicated: error bars represent mean \pm standard deviation. $n = 12$ for each condition. One-way ANOVA p -value < 0.01 . One-way ANOVA with Šidák-adjusted p -values for comparison to control: > 0.05 (vs. 1 nM); < 0.05 (vs. 10 nM); < 0.05 (vs. 100 nM); < 0.05 (vs. 1 μ M); and < 0.01 (vs. 10 μ M). For numerical values of data, see Excel Table S2. (C) Representative FACS contour plots showing distribution of live-gated events. First row indicates cell staining profile following incubation with DAPI and proliferation, measured using anti-BrdU antibody following a 30-min pulse with the thymidine analogue BrdU. Second row indicates distribution of proliferating cells labeled with anti- γ H2AX antibody, a marker of DNA damage. Third panel indicates distribution of cells labeled with γ H2AX antibody and anti-cPARP antibody, a marker of apoptosis. Numbers indicate proportion of live-gated events within the regions indicated. (D–I) Scatter-bar plots indicating proportion of live-gated events in the different populations indicated. Data indicate mean \pm standard deviation. $n = 12$ –15. For complete set of one-way ANOVA and calculated one-way ANOVA with Šidák-adjusted p -values for each treatment condition compared with control, see Table 1. For numerical values of data, see Excel Table S7. Note: ANOVA, analysis of variance; β FGF, basic fibroblast growth factor; BPA, bisphenol A; DAPI, 4',6-diamidino-2-phenylindole; ESC, embryonic stem cell; EpiLC, epiblast-like cell; FACS, fluorescence-activated cell sorting; LIF, leukemia inhibitory factor; KSR, knockout serum replacement. Number of asterisks on plots indicate level of statistical significance: * ($p < 0.05$); ** ($p < 0.01$); *** ($p < 0.001$).

“Intracellular Staining” section) and DAPI-incorporation in cells pulsed with BrdU (10 μ M) 30–60 min prior to cell harvesting; and by proliferation tracing using cells loaded with CellTrace™ Yellow (5 μ M, loaded for 20 min at 37°C, protected from light) (ThermoFisher Scientific). This dye passively diffuses through the cell membrane, where it remains covalently bound to intracellular amines, resulting in a stable, well-retained fluorescent signal with no/low cellular toxicity (Tempny 2018). Cell division results in a progressive diminution of signal intensity, which can be used to

estimate the number of cell divisions a cell has undergone. To calculate numbers of cell division, the Proliferation Platform on FlowJo™ software was used (version 10; FlowJo, LLC).

Flow Cytometry

For purification of PGCLCs from day-5 aggregates, TrypLE™ Select–dissociated cells [incubated for 8 min at 37°C with agitation (950 rpm) on a Thermomixer (Eppendorf)] were resuspended

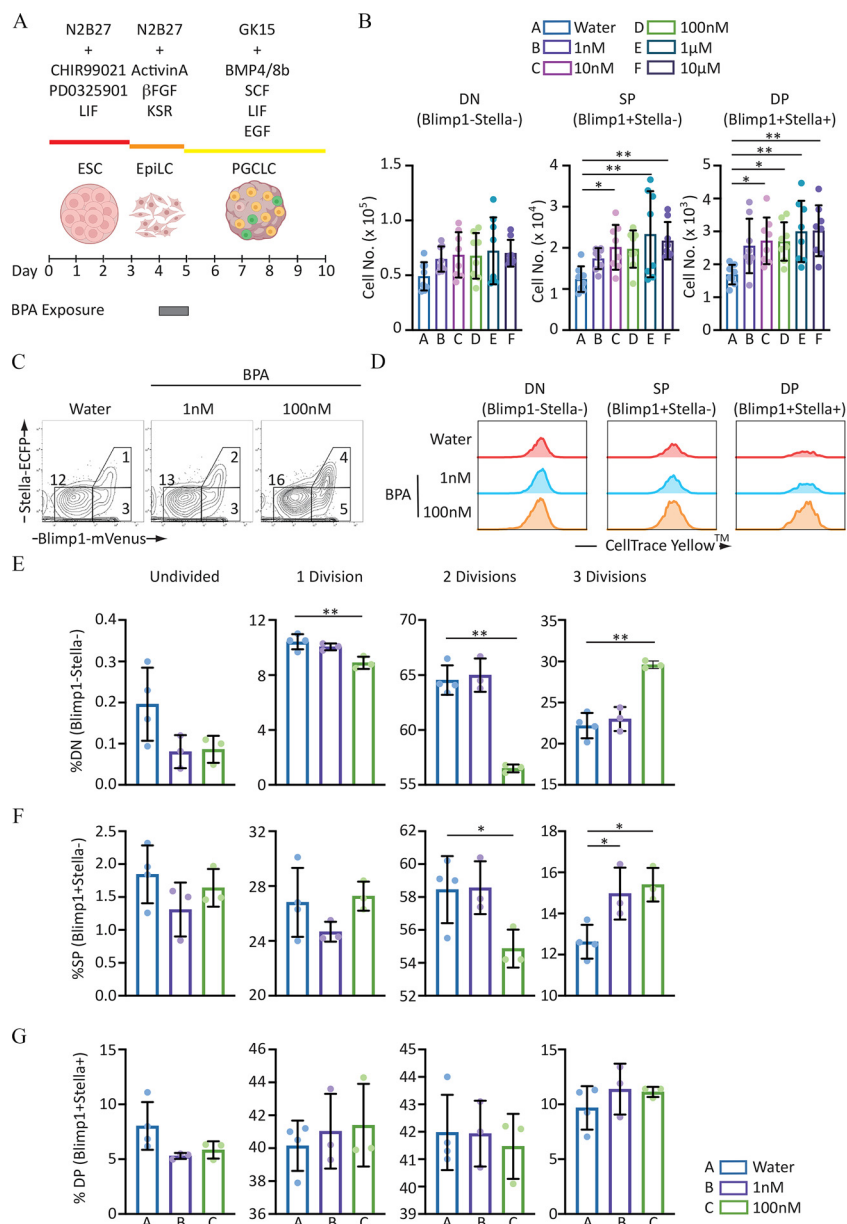


Figure 2. Proliferation analysis of different cell populations in day 5 aggregates derived from EpiLCs following 24-h BPA exposure. (A) Graphic illustrating BPA exposure and cell differentiation strategy. Uncolored cells represent Blimp1⁻; Stella⁻/DN/nongerm cells; yellow cells represent Blimp1⁺/presumed transitioning germ cells; green cells represent Blimp1⁺; Stella⁺/DP/BVSC/d5 PGCLCs. [Illustration in part created with ©BioRender (biorender.com), per the Biorender terms and conditions.] (B) Scatter-bar plots showing absolute numbers of cells in the different gated subpopulations indicated following exposure of EpiLCs to different BPA concentrations indicated. Plots represent mean \pm standard deviation. $n = 8$. For calculated one-way ANOVA with Sidák-adjusted p -values for comparison to control and cell numbers, see Table 2 and Excel Table S8, respectively. (C) FACS contour plots showing cell populations indicated from d5 aggregates. EpiLCs were treated with the conditions indicated for 24 h prior to aggregate formation. (D) Representative histograms showing CellTrace™ Yellow staining profile of the different cell populations indicated. The Y-axis represents the number of cells, whereas the X-axis represents the fluorescence intensity. Recurring cell divisions create the appearance of secondary peaks, which widens the original peak of undivided cells. (E–G) Scatter-bar plots showing proportion of cells in the different populations indicated that remain undivided or have undergone one, two, or three cell divisions in day 5 aggregates. Number of divisions calculated using FlowJo Proliferation tool (version 10; FlowJo, LLC). Scatter plots show mean \pm standard deviation. $n = 3–4$. For calculated one-way ANOVA with Sidák adjusted p -values for comparison and cell proportions, see Table 3 and Excel Table S11, respectively. Note: ANOVA, analysis of variance; β FGF, basic fibroblast growth factor; BMP4, bone morphogenetic protein 4; BMP8b, bone morphogenetic protein 8b; BPA, bisphenol A; BVSC, B lymphocyte-induced maturation protein 1 *Blimp1-mVenus* and *Stella-ECFP* reporter transgenes; DAPI, 4',6'-diamidino-2-phenylindole; DN, double negative; DP, double positive; EGF, epidermal growth factor; ESC, embryonic stem cell; EpiLC, epiblast-like cell; FACS, fluorescence-activated cell sorting; LIF, leukemia inhibitory factor; KSR, knockout serum replacement; PGC, primordial germ cell; PGCLC, PGC-like cell; SP, single positive.

in cell sort buffer [$1 \times$ Dulbecco's phosphate buffered saline (DPBS), 1% BSA, 1 mM EDTA, 25 mM HEPES], passed through a cell strainer (70 μ m), and sorted on a BD FACSAria III (BD Biosciences), gating and collecting cell populations of interest in Eppendorf tubes containing GK15 media. Purified cells were used for the extraction of total RNA and subsequent library

construction (see below). For analysis, cells were resuspended in fluorescence-activated cell sorting (FACS) buffer ($1 \times$ DPBS, 2% BSA, 1 mM EDTA, 25 mM HEPES, 100 U/mL penicillin, 0.1 mg/mL streptomycin, 2 mM L-glutamine), and analyzed on an LSR II (BD Biosciences). Cells were initially identified by forward- and side-scatter gating, with back-gating used to verify the

accuracy by which target cell populations were identified. Cell populations of interest were identified by 2-D plots displaying the parameter of interest. Manually defined gates as well as quadrants were used, as indicated. For positive controls to show the presence of DNA damage and apoptosis, v6.5 ES cells were treated with etoposide (10 μ M; E1383; Sigma-Aldrich) and doxorubicin (500 nM; 44583; Sigma-Aldrich), both dissolved in DMSO, for 12 h prior to harvesting, fixing, and staining.

Intracellular Staining

Cells were permeabilized, fixed, and stained using the Apoptosis, DNA Damage and Cell Proliferation Kit (BD Biosciences) according to the manufacturer's protocol. In summary, cells were harvested and pelleted by centrifugation [5 min, 300 relative centrifugal force (rcf)]. Typically, between 2×10^5 and 5×10^5 cells were collected for each staining experiment. Pelleted cells were fixed in 100 μ L BD Cytofix™/Cytoperm™ fixation/permeabilization solution before incubating on ice for 30 min. Cells were then washed with 100 μ L $1 \times$ BD Perm/Wash™ buffer (BD Biosciences) and pelleted by centrifugation. Following aspiration of supernatant, cells were resuspended in 100 μ L BD Cytofix™/Cytoperm™ Plus permeabilization buffer and incubated on ice for 10 min. Cells were then washed with 100 μ L $1 \times$ BD Perm/Wash™ buffer (BD Biosciences) and pelleted by centrifugation. Following aspiration of supernatant, cells were resuspended in 100 μ L BD Cytofix™/Cytoperm™ fixation/permeabilization solution before incubating on ice for 5 min. Cells were then washed with 100 μ L $1 \times$ BD Perm/Wash™ buffer and pelleted by centrifugation. Following aspiration of supernatant, cells were resuspended in 50 μ L $1 \times$ BD Perm/Wash™ buffer supplemented with 150 μ g/mL DNase I and incubated at 37°C for 1 h. Following incubation, cells were washed in 150 μ L $1 \times$ BD Perm/Wash™ buffer and pelleted by centrifugation. Following aspiration of supernatant, cells were resuspended in 30 μ L of $1 \times$ BD Perm/Wash™ buffer containing antibodies [2 μ L of each of anti-BrdU PerCP-Cy5.5 (clone 3D4); anti- γ -H2AX AF 647 (clone N1-431); and anti-cleaved poly(ADP-ribose) polymerase (cPARP) (Asp214) PE (clone F21-852), for a final antibody dilution of 1:15]. All antibodies were derived from BD Biosciences as part of the Apoptosis, DNA Damage and Cell Proliferation Kit. Cells were incubated in the dark for 20 min, before washing with 180 μ L $1 \times$ BD Perm/Wash™ buffer and pelleting by centrifugation. Following aspiration of supernatant, cells were resuspended in 300 μ L of $1 \times$ BD Perm/Wash™ buffer with DAPI (final concentration 1 μ g/mL DAPI). Cells were kept at 4°C and shielded from light until ready for analysis.

Total RNA Extraction

RNA was extracted from cell pellets (fresh or thawed snap-frozen) by using either an AllPrep DNA/RNA Mini or Micro Kit (Qiagen), according to the manufacturer's protocol. RNA concentration was measured using a NanoDrop™ 2000 UV spectrophotometer (ThermoFisher Scientific).

RNA-Seq Library Construction

Strand-specific RNA-seq libraries were prepared with Universal Plus mRNA-Seq kit (Nugen), according to the manufacturer's protocol. Briefly, this process consisted of poly(A) RNA selection, RNA fragmentation, and double-stranded cDNA generation using a mixture of random and oligo(dT) priming, followed by end repair to generate blunt ends, adaptor ligation, strand selection, and polymerase chain reaction (PCR) amplification to produce the final library. Different index adaptors were used for multiplexing samples in one sequencing lane. Sequencing

was performed on Illumina HiSeq 3000 and NovaSeq 6000 sequencers for paired end (PE), 2×150 base pair (bp) runs. Data quality check was performed using Illumina Sequencing Analysis Viewer (SAV) software. Demultiplexing was performed with Illumina Bcl2fastq2 program (version 2.19.1.403; Illumina Inc.).

Expression Analysis of RNA-Seq Data

Fastq reads were checked for overall quality by FastQC (<https://www.bioinformatics.babraham.ac.uk/projects/fastqc/>). For differential gene expression analysis, reads were aligned using STAR (Dobin et al. 2013) with the following commands: STAR --runThreadN 20 --readFilesCommand zcat --runMode alignReads --outFilterMultimapNmax 1 --outSAMtype BAM Unsorted --quantMode GeneCounts --twopassMode Basic. After sorting, indexing and converting into SAM file format using SAMtools (Li et al. 2009), read counts were obtained using HTSeq (<https://htseq.readthedocs.io/en/master/>) with the following commands: htseq-count --mode=union --stranded=no --idattr=gene_id -r pos -f sam. Output files were filtered to remove genes with nine or fewer read counts. These were then used for differential gene expression analysis using the edgeR Bioconductor package (<https://bioconductor.org/packages/release/bioc/html/edgeR.html>). Gene counts were normalized using the trimmed mean of *M*-values normalization (TMM) method (Robinson and Oshlack, 2010) before determining counts per million (cpm) values. For a gene to be classified as showing differential expression between treated and untreated germ cells, a threshold fold-change of ≥ 2 and Benjamini-Hochberg adjusted $p \leq 0.05$ had to be met.

For analysis of X-linked gene expression levels, genes were binned based on chromosomal location, before determining median expression levels for each chromosome. Median expression for all autosomal genes (all chromosomes except X) was determined and then used to normalize the median expression level for all chromosomes.

For analysis of repeat expression, fastq files were aligned using HiSat2 (Kim et al. 2019) with the -k parameter set to allow up to 100 alignments. Resultant sam files were then used to generate read counts for repeats using TETools (Lerat et al. 2017) and a mouse-specific repeat reference file generated using RepeatMasker. For each biological repeat between conditions (untreated and exposed), total numbers of reads following alignment using TETools was determined before down sampling of aligned sam files to ensure that an equivalent number of reads was analyzed across all samples. For an element to be considered differentially expressed between untreated and exposed samples, there needed to be 10 or more reads aligning to the repeat in either or both conditions, as well as a two-fold or greater difference in read number. Fastq files and Excel table showing trimmed mean of *M*-values (TMM)-normalized cpm of genes ≥ 10 reads are accessible via the Gene Expression Omnibus (GEO), accession number GSE157570.

Gene Ontology (GO) Analysis and CirGO Plot Generation

Lists of differentially expressed genes as well as a list of all genes analyzed were generated from read counts using edgeR Bioconductor package (Robinson et al. 2010). Enrichment of GO terms in lists of up- and down-regulated genes was determined using Gene Ontology enRlchment anaLysis and visualiZation tool (GORilla, <http://cbl-gorilla.cs.technion.ac.il>) (Eden, 2009). Redundant GO terms were removed using reduce + visualize gene ontology (REVIGO, <http://revigo.irb.hr>) (Supek et al. 2011) to generate .csv files. These were then used to generate Circular Gene Ontology (CirGO) plots using the open source CirGO software

Table 1. Calculated *p*-values for differences in cell populations in BPA-exposed EpiLCs. Data refer to Figure 1.

| Cell population | ANOVA | Šidák-adjusted ANOVA | | | | |
|--|----------------|----------------------|-------------------|--------------------|------------------|-------------------|
| | | Control vs. 1 nM | Control vs. 10 nM | Control vs. 100 nM | Control vs. 1 μM | Control vs. 10 μM |
| Late apoptotic | 0.0083 (**) | 0.2824 | 0.0361 (*) | 0.0173 (*) | 0.0167 (*) | 0.0256 (*) |
| S-phase/M | 0.0004 (***) | 0.3018 | 0.0483 (*) | 0.0142 (*) | 0.0064 (**) | 0.0137 (*) |
| BrdU ⁺ γ-H2AX ⁺ | 0.0113 (*) | 0.425 | 0.0778 | 0.0215 (*) | 0.0151 (*) | 0.0116 (*) |
| γ-H2AX ⁺ | 0.0294 (*) | 0.4879 | 0.0536 | 0.025 (*) | 0.0217 (*) | 0.0172 (*) |
| cPARP ⁻ γ-H2AX ⁺ | 0.0005 (***) | 0.22 | 0.0521 | 0.004 (**) | 0.0024 (**) | 0.0002 (***) |
| cPARP ⁺ γ-H2AX ⁺ | <0.0001 (****) | 0.0432 | 0.0021 (**) | 0.0008 (***) | 0.0017 (**) | 0.0014 (**) |

Note: Number of asterisks indicate level of statistical significance: * (*p* < 0.05); ** (*p* < 0.01); *** (*p* < 0.001); **** (*p* < 0.0001). BPA, bisphenol A; EpiLC, epiblast-like cell.

(version 1.0; <https://github.com/IrinaVKuznetsova/CirGO.git>) (Kuznetsova 2019). Terms were included if the Benjamini-Hochberg-adjusted *p*-value was less than 0.05.

Statistical Methods

For analysis of proliferation and cell staining data, calculated one-way analysis of variance (ANOVA) was initially performed, followed by Holm-Šidák testing for pairwise comparison between exposed and water/untreated control samples. For differential gene expression analysis, adjusted *p*-values were calculated using the Benjamini-Hochberg method. For statistical analysis of gene expression data derived from differential expression of RNA-seq data, Wilcoxon-signed rank test was used. In all cases, significance was determined by *p*-values less than or equal to 0.05. For analysis of repeat representation, chi-square analysis was performed. For each experiment, unless otherwise noted, technical *n* = 3.

Results

Cell Proliferation and Viability Analysis of BPA-Exposed Murine EpiLCs

Because our exposure window corresponds to the stage of EpiLCs prior to PGCLC differentiation, we first examined the consequences of BPA exposure on EpiLCs. Exposure of these cells for 24 h resulted in a significantly higher number of cells recovered, which was in a concentration-dependent manner (Figure 1B; *p* = 0.0086, one-way ANOVA, and Excel Table S2). By contrast, exposure of BVSC ESCs to BPA for up to 48 h had no significant effect on the number of cells recovered (Figure S2; *p* = 0.62, one-way ANOVA, and Excel Table S3). To determine the generality of BPA's effect on cell number in EpiLCs, we also examined two additional male (XY) ESC clones, v6.5 and BVSC-R8 (Figure S3 and Excel Table S4). An interesting finding was that we did not detect any significant difference in cell number recovered when comparing unexposed to BPA-exposed cells over a range of different concentrations. This extended to the lack of perturbation in cell number in day 5 (d5) aggregates generated from BVSC-R8, (Figure S4A and Excel Table S5). Transcriptome analysis revealed an absence of differentially expressed genes between BVSC-R8 PGCLCs derived from untreated and 100-nM BPA-exposed EpiLCs (Figure S4B and Excel Table S6). We found it interesting that d5 PGCLCs derived from BVSC-H18 and BVSC-R8 displayed a marked difference in their transcriptional identity, despite

showing no significant difference in their expression of germ cell markers associated with the PGCLC state (Figure S4B and S4C).

The higher number of BVSC-H18 cells recovered when exposed at the EpiLC stage could be accounted for by a higher rate of proliferation, lower apoptosis levels, or a combination of both. To investigate the mechanisms involved, we performed intracellular staining and analysis by flow cytometry. Because BPA exposure has previously been reported to result in DNA damage in germ cells (Barbonetti et al. 2016; Sahu et al. 2020; Yin et al. 2020), we also examined the proportion of cells staining positive for γH2AX, a marker of DNA damage (Rogakou et al. 1998). To control for the ability to detect γH2AX and cPARP signals, separate samples of EpiLCs were also exposed to the DNA-damaging agent etoposide (10 μM), the cytotoxin doxorubicin (500 nM), or both (Figure S5). Analysis of BrdU and DAPI incorporation revealed that BPA exposure resulted in the presence of a significantly higher proportion of cells in S-phase/M, which occurred in a concentration-responsive manner (Figure 1C and D; *p* = 0.0181, one-way ANOVA; Table 1 and Excel Table S7). Analysis of either BrdU with DAPI incorporation or detection of cleaved PARP (cPARP, a marker of early apoptosis), revealed a significantly higher proportion of cells undergoing apoptosis (Figure 1C, E, and I; *p* = 0.0095, and 0.0002, respectively, one-way ANOVA; Table 1 and Excel Table S7). Examination of live events that were positive for γH2AX revealed the presence of a significantly higher proportion of cells with DNA damage in response to BPA exposure (Figure 1C and F; *p* = 0.029, one-way ANOVA; Table 1 and Excel Table S7). We were surprised to observe a significantly higher proportion of both viable and proliferating cells with DNA damage (Figure 1C, G, and H; *p* = 0.0015 and *p* = 0.02, respectively; Table 1 and Excel Table S7).

Proliferation Analysis of PGCLCs Derived from BPA-Exposed EpiLCs

We next investigated whether the brief exposure of EpiLCs to BPA had consequences on induction of PGCLCs in day 5 (d5) aggregates (Figure 2A). During PGCLC induction, expression of the Blimp1-mVenus (BV) reporter is initially up-regulated before the Stella-ECFP (SC) reporter, allowing discrimination of three different cell populations: Blimp1⁻; Stella⁻ (double negative, DN), Blimp1⁺; Stella⁻ (single positive, SP), and finally PGCLCs that are Blimp1⁺; Stella⁺ (double positive, DP). In all induction experiments, equal numbers of control or exposed cells were

Table 2. Calculated *p*-values for differences in cell populations in PGCLCs derived from BPA-exposed EpiLCs.

| Cell population | ANOVA | Šidák-adjusted ANOVA | | | | |
|-----------------|----------------|----------------------|-------------------|--------------------|------------------|-------------------|
| | | Control vs. 1 nM | Control vs. 10 nM | Control vs. 100 nM | Control vs. 1 μM | Control vs. 10 μM |
| DN | <0.0001 (****) | 0.1892 | 0.0766 | 0.0399 (*) | 0.0287 (*) | 0.0513 |
| SP | 0.0013 (**) | 0.232 | 0.025 (*) | 0.0155 (*) | 0.001 (**) | 0.0054 (**) |
| DP | 0.004 (**) | 0.1559 | 0.0576 | 0.0475 (*) | 0.0071 (**) | 0.006 (**) |

Note: Data refers to Figure 2. *n* = 12–15. ANOVA, analysis of variance; BPA, bisphenol A; EpiLC, epiblast-like cell; DN, double negative (Blimp1⁺; Stella⁻); DP, double positive (Blimp1⁺; Stella⁺) PGC, primordial germ cell; PGCLC, PGC-like cell; SP, single positive (Blimp1⁺; Stella⁻). Number of asterisks indicate level of statistical significance: * (*p* < 0.05); ** (*p* < 0.01); *** (*p* < 0.001); **** (*p* < 0.0001).

seeded at the start of each induction phase (see “Methods” section). Cell populations analyzed were initially identified using a “live” cell gate, based on forward- and side-scatter profiles. When measuring absolute numbers of events, BPA exposure of EpiLCs resulted in the presence of significantly higher numbers of SP and DP cells in d5 aggregates, (Figure 2B and Table 2; $p=0.0084$; $p=0.0071$ for SP and DP, respectively, one-way ANOVA and Excel Table S8). As a proportion of all live events, significantly higher levels were observed for DN and SPs (Figure S6 and Excel Table S9 and S10; $p=0.0045$ and 0.013 , respectively, one-way ANOVA). For PGCLCs, higher numbers of cells were observed when derived from EpiLCs exposed to 10 nM BPA or above (Figure 2B,C; Excel Table S8). In addition to the aforementioned methods of measuring proliferation, to further investigate the proliferative kinetics of the three different cell populations, we also used proliferation tracing of EpiLCs preloaded with CellTrace™ Yellow dye on day 0 of aggregate formation. This assay revealed that a greater proportion of DN cells had undergone three mitotic divisions, with concomitant reductions in the proportion of cells that had undergone either only one or two divisions (Figure 2E; $p=0.0059$, 0.0001 , and 0.0003 , calculated one-way ANOVA with Sidák-adjusted p -value, control vs. 100 nM, one, two, and three divisions, respectively; Table 3; Excel Table S11). A greater proportion of SP cells derived from EpiLCs exposed to BPA underwent three mitotic divisions, compared to control (Figure 2C, D, and F; $p=0.013$, one-way ANOVA; Table 3; Excel Table S11). Although not significant, there was a similar trend for a higher proportion of DP/PGCLCs that had undergone three mitotic divisions (Figure 2C, D, and G; Table 3; Excel Table S11).

Assessment of Gene Expression Differences in PGCLCs Derived from EpiLCs Exposed to BPA

Because differences in EpiLC and, subsequently, PGCLC behavior were observed at a concentration of 100 nM, we examined the nature of any underlying transcriptional alterations using RNA-seq at this concentration (Figure 3A). When compared to EpiLCs exposed to vehicle (water) control, unsupervised differential gene expression analysis of the transcriptome of EpiLCs exposed to 100 nM BPA revealed an absence of differentially expressed genes (Excel Table S12). However, as we observed that BPA exposure resulted in a higher proportion of EpiLCs labeling positive for γ H2AX and a lower proportion of cells showing signs of apoptosis, we also performed a targeted analysis of the expression of

genes in GO Biological Process-terms associated with either DNA damage or apoptosis to determine whether our transcriptome data could provide some insight into any potential mechanisms involved (Figure S7 and Excel Table S13). For apoptosis-associated GO terms, nine GO terms showed significant differences between control and exposed samples (Figure S7A and Excel Table S13). As well as higher median expression levels of GO terms associated with positive regulation of apoptosis (e.g., GO:0,043,065, positive regulation of apoptotic process), there was also higher expression of genes in one GO term associated with negative regulation of apoptosis (GO:2,001,237, negative regulation of extrinsic apoptotic signaling pathway). For GO terms associated with DNA damage, there was higher expression in 10 GO terms associated with checkpoint control of DNA damage (Figure S7B and Excel Table S13).

We next examined the transcriptome of PGCLCs derived from EpiLCs that were either untreated or exposed to 100 nM BPA. Expression profiling of known markers of PGCLC-identity revealed no significant differences between PGCLCs derived from control or 100 nM BPA-exposed EpiLCs (Figure 3B; $p=0.1324$, Wilcoxon matched pairs signed rank test). However, transcriptome analysis globally using principal component analysis (PCA) indicated a clear divergence between control and exposed cells (Figure 3C). Analysis of differentially expressed genes using stringent conditions (fold-change ≥ 2 ; False Discovery Rate (FDR) ≤ 0.05) revealed that although 161 genes were down-regulated (Figure 3D; Excel Table S14), the majority of genes (501) were up-regulated (Figure 3D; Excel Table S15). Examples of down- and up-regulated genes are shown in Figure 3E.

To investigate biological functions/pathways affected in control and exposed germ cells, gene ontology analysis of enriched Biological Process terms was performed. Up-regulated genes were enriched in biological processes, such as ion and lipid transport [e.g., GO:0006811 (ion transport)]; GO:0006869 (lipid transport), lipoprotein metabolism [e.g., GO:0042157 (lipoprotein metabolic process)] and steroid metabolism [e.g., GO:0008202 (steroid metabolic process)] (Figure 4; Excel Table S16 and S17). We also noted that enriched terms in the GO Cellular Component category featured proteins associated with the extracellular space and cell membrane (Figure S8).

BPA-Induced Perturbations in Gene Expression in PGCLCs

We determined whether genes associated with retinoic acid biosynthesis and/or signaling showed altered expression in PGCLCs derived from exposed EpiLCs. There was higher expression of genes in two gene ontology terms associated with retinoic acid biosynthesis: GO: 0042573 (retinoic acid metabolic process) and GO: 0042572 (retinol metabolic processes) (Figure 5A,B; Figure S9A and 9B). Expression levels of genes containing a Retinoic Acid Response Element (RARE, Lalevée et al. 2011) and therefore inferred to be targets of retinoic acid signaling were found to be higher (Figure 5C; Figure S9C, Wilcoxon-signed rank test $p=0.0022$). An interesting finding was that although expression of *Strad8* was not significantly different, there was a trend toward lower levels in exposed cells (Figure S9D). Examination of whether BPA-exposure of EpiLCs had any impact on nuclear hormone receptor (NHR) expression levels in PGCLCs had revealed that neither retinoic acid nor estrogen nuclear receptor family members were significantly altered (Figure S9E). Despite the lack of any differences in the expression of RA and estrogen nuclear receptor family members, differential gene expression analysis revealed two NHRs that were up-regulated: these were *Hepatocyte nuclear factor 4 alpha (Hnf4a)* and *Nuclear receptor subfamily 2 group f member 2 (Nr2f2)* (Excel Table S18).

Table 3. Calculated p -values for differences in cell populations in PGCLCs derived from BPA-exposed EpiLCs.

| Cell population | ANOVA | Šidák-adjusted ANOVA | |
|-----------------|----------------|----------------------|--------------------|
| | | Control vs. 1 nM | Control vs. 100 nM |
| DN_Undivided | 0.0159 (*) | 0.0775 | 0.0954 |
| DN_Div1 | <0.0001 (****) | 0.6194 | 0.0023 (**) |
| DN_Div2 | <0.0001 (****) | 0.9434 | <0.0001 (****) |
| DN_Div3 | <0.0001 (****) | 0.7819 | <0.0001 (****) |
| SP_Undivided | 0.1791 | 0.2317 | 0.8561 |
| SP_Div1 | 0.0052 (**) | 0.3008 | 0.9754 |
| SP_Div2 | 0.0293 (*) | 0.9995 | 0.0394 (*) |
| SP_Div3 | <0.0001 (****) | 0.0325 (*) | 0.0129 (*) |
| DP_Undivided | 0.0263 (*) | 0.0724 | 0.1703 |
| DP_Div1 | 0.0005 (****) | 0.9138 | 0.7967 |
| DP_Div2 | 0.0054 (**) | >0.9999 | 0.9552 |
| DP_Div3 | 0.0031 (**) | 0.57 | 0.6803 |

Note: Data refer to Figure 2. $n=3-4$. BPA, bisphenol A; DN, double negative (Blimp1-; Stella-); DP, double positive (Blimp1+; Stella+); EpiLC, epiblast-like cell; PGC, primordial germ cell; PGCLC, PGC-like cell; SP, single positive (Blimp1+; Stella+). Number of asterisks indicate level of statistical significance: * ($p < 0.05$); ** ($p < 0.01$); *** ($p < 0.001$); **** ($p < 0.0001$).

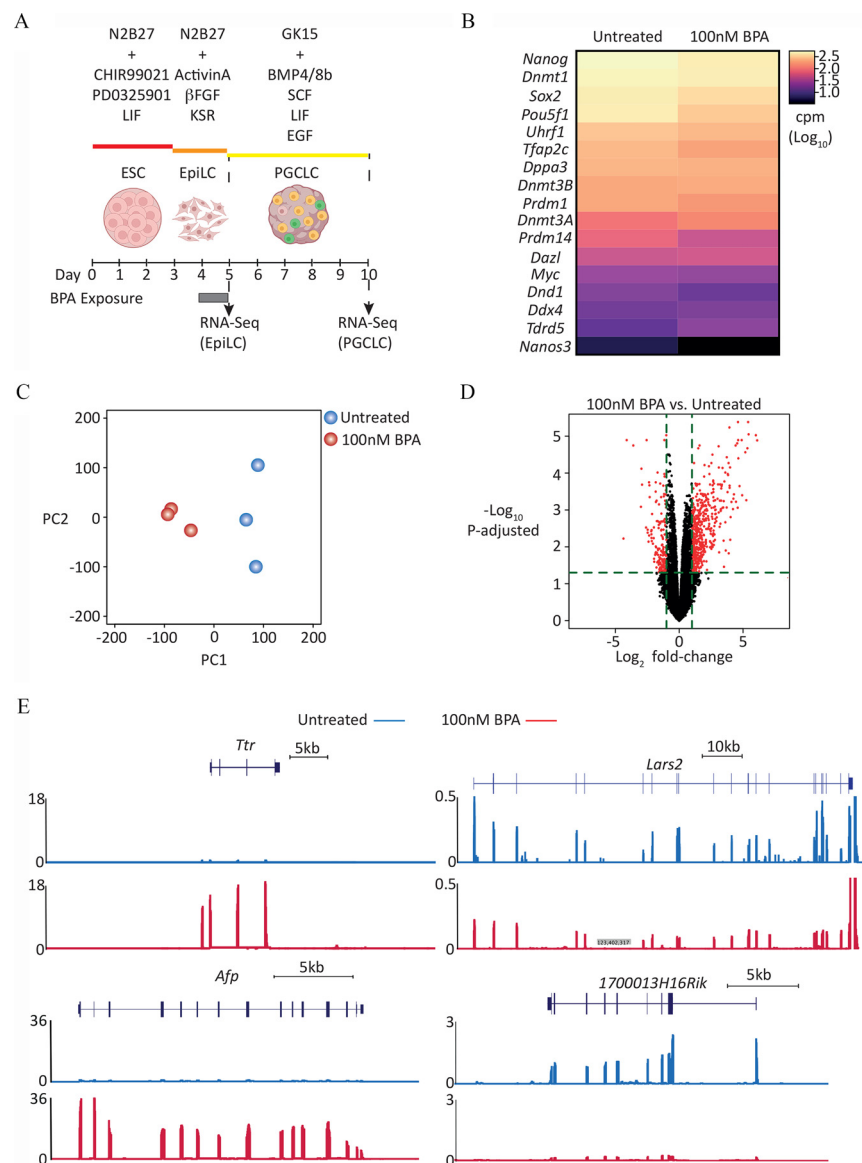


Figure 3. Transcriptome analysis of PGCLCs derived from EpiLCs exposed to BPA. (A) Graphic showing dosing and differentiation strategy followed by cell collection for RNA-seq library generation. Uncolored cells represent Blimp1⁻; Stella⁻/DN/nongerm cells; yellow cells represent Blimp1⁺; Stella⁻/SP/presumed transitioning germ cells; green cells represent Blimp1⁺; Stella⁺/DP/BVSC/d5 PGCLCs. [Illustration in part created with ©BioRender – (biorender.com), per the Biorender terms and conditions.] (B) Log₁₀-expression level-ranked heatmap of germ cell markers indicated in RNA-seq data generated from d5 aggregate FACS-purified DP/PGCLCs, derived from EpiLCs exposed to control (untreated) or 100 nM BPA. Candidate germ cell marker list taken from Hayashi et al. (Hayashi et al. 2011). (C) PCA of transcriptome of d5 DP/BVSC cells, derived from untreated or 100 nM BPA-exposed EpiLCs. (D) Volcano plot of RNA-seq data displaying gene expression pattern of d5 DP/PGCLCs, derived from untreated or 100 nM BPA-exposed EpiLCs. Significant differentially expressed genes (log₂-fold change ≥ 2, Benjamini-Hochberg-adjusted *p* ≤ 0.05) are highlighted in red. (E) Genome browser view of expression data for representative genes, up- (Ttr and Afp) and down-regulated (Lars2 and 1700013H16Rik) in d5 DP/BVSC cells, derived from 100 nM BPA-exposed EpiLCs. Y-axis values are normalized cpm/10³. For each locus, top panel represents “Untreated” and bottom panel represents “100nM BPA exposed.” For full list of differentially up- and down-regulated genes, see Excel Tables S14 and S15, respectively. Note: βFGF, basic fibroblast growth factor; BMP4, bone morphogenetic protein 4; BMP8b, bone morphogenetic protein 8b; BPA, bisphenol A; BVSC, B lymphocyte-induced maturation protein 1 Blimp1-mVenus and stella-ECFP reporter transgenes; cpm, counts per million; DN, double negative; DP, double positive; EGF, epidermal growth factor; embryonic stem cell; EpiLC, epiblast-like cell; FACS, fluorescence-activated cell sorting; KSR, knockout serum replacement; LIF, leukemia inhibitory factor; PGC, primordial germ cell; PGCLC, PGC-like cell; SCF, stem cell factor.

Analysis of meiosis-specific gene ontology terms revealed lower expression of genes associated with several meiotic biological processes: GO:0051321 (meiotic cell cycle) and GO:1901993 (regulation of meiotic cell cycle phase transition) (Figure 5D–G; Table 4; Excel Table S19 and Figure S10). However, other meiosis-specific GO terms revealed no significant differences resulting from BPA exposure (Figure S11 and Excel Table S20).

Remarkably, among down-regulated genes, enrichment for transcripts associated with gametogenesis was observed (Excel Table S21). Several genes are members of the *X-linked*,

lymphocyte regulated (Xlr) family, which generate coding and noncoding transcripts that are highly expressed in meiotic germ cells (Garchon et al. 1989; Shi et al. 2013). Of the 65 annotated *Xlr* family members listed in the latest build of the *Mus musculus* genome (GRCm38/mm10), 7 were found to be expressed and significantly lower in d5 PGCLCs derived from BPA-exposed EpiLCs (Figure 5H; Wilcoxon-signed rank test *p* = 0.0005). In addition, we noted that a substantial proportion, 25% (40 of 161) of down-regulated genes were X-linked, including the long noncoding RNA (lncRNA), *X-inactive specific transcript (Xist)* (Figure 5I). We

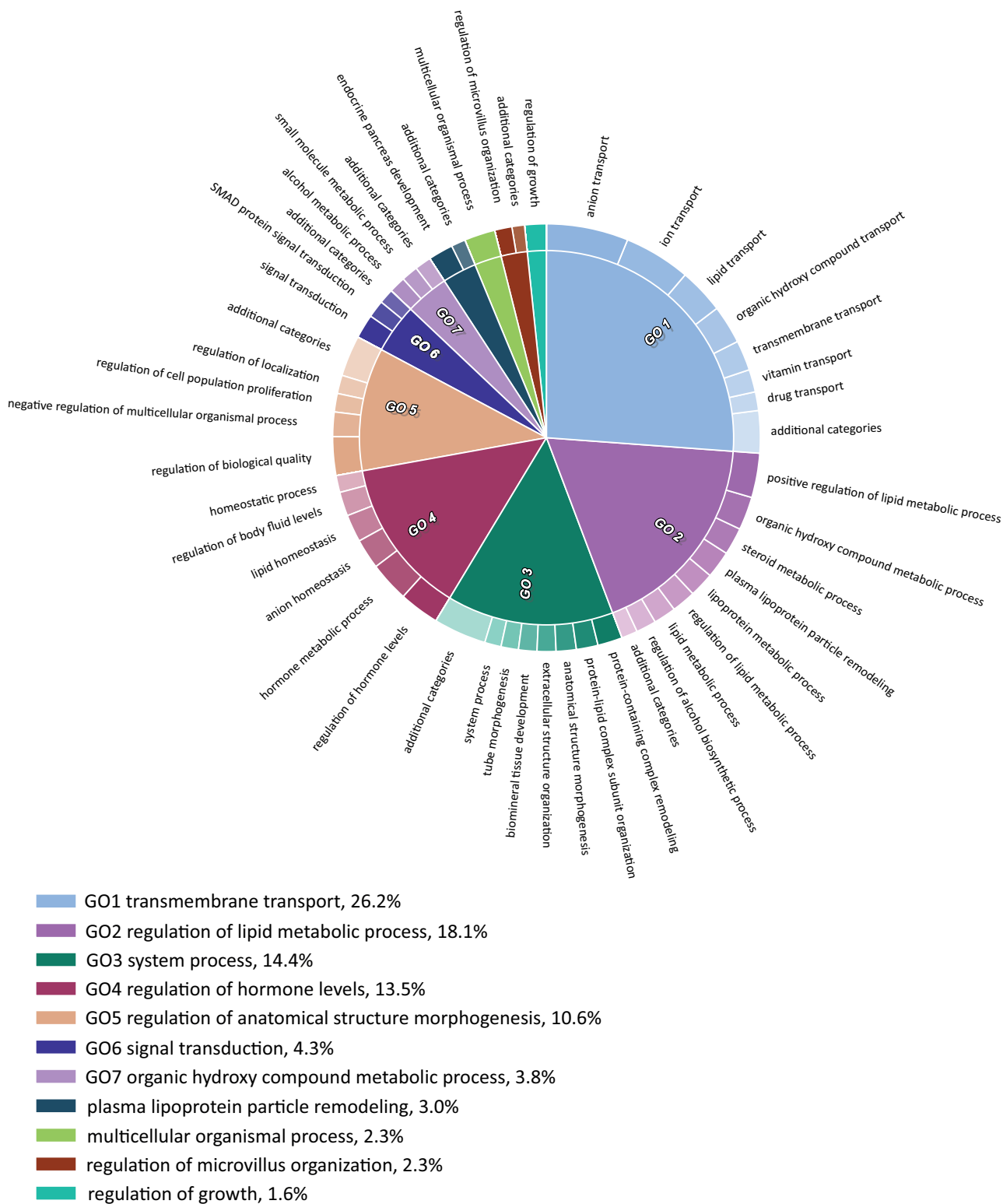


Figure 4. GO biological processes categories enriched in genes up-regulated in day 5 (d5) DP/ PGCLCs, derived from 100 nM BPA-exposed EpiLCs. CirGO plots showing parent representative records (inner ring) and child, description records (outer ring). For calculated *p*-values, see Excel Table S17. Note: BPA, bisphenol A; DP, double positive; EpiLC, epiblast-like cell; GO, gene ontology; PGC, primordial germ cell; PGCLC, PGC-like cell.

also examined whether global levels of expression of X-linked genes relative to those on autosomes were affected. Comparison of expression values by chromosome, normalized by global median expression of all autosomal genes, in each sample revealed that BPA-exposed germ cells had significantly lower expression of

X-linked genes (Figure 5J; Benjamini-Hochberg-adjusted $p < 0.05$). In addition, this analysis revealed that BPA-exposure also resulted in lower expression of genes located on chromosomes 12 and higher expression of genes on chromosomes 1, 8, and 19 (Figure 5J; Benjamini-Hochberg-adjusted $p < 0.05$).

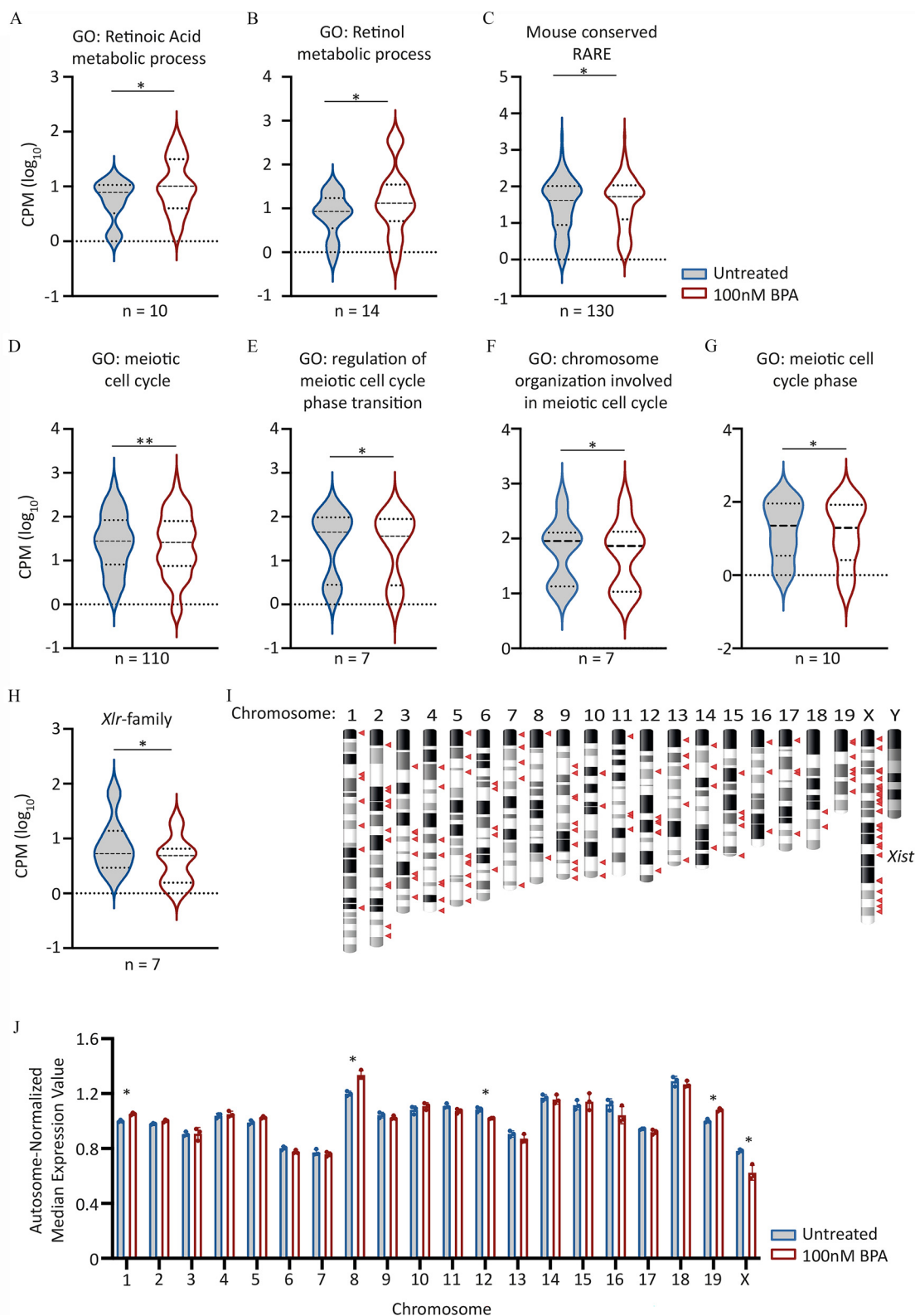


Figure 5. Candidate gene expression analysis in day 5 (d5) PGCLCs derived from EpiLCs exposed to 100 nM BPA. (A–H) Violin plots showing aggregated expression levels (\log_{10} cpm) for the different gene sets listed. Lines indicate median and quartiles. For Wilcoxon matched pairs signed rank test p -values, see Table 4. GO biological process terms listed were obtained from http://www.informatics.jax.org/vocab/gene_ontology/GO:0.008.150. Genes within 10 kb of RAREs, and conserved between *Mus musculus* genome and at least six other different species, including humans were obtained from Lalevée et al. (Lalevée et al. 2011). For full lists of genes analyzed expression values and p -values, see Excel Tables S18–S21. (I) Chromosome ideogram indicating chromosome location of down-regulated genes in d5 PGCLCs derived from BPA-exposed EpiLCs. Down-regulated genes defined as those with a fold change of >2 and Benjamini-Hochberg-adjusted $p < 0.05$. Genes indicated by red triangles. (J) Scatter-bar plot showing autosome-normalized mean expression values for genes binned by chromosome. Median gene expression values for each chromosome was determined before normalizing by total autosomal gene expression value. Asterisks indicate chromosomes with differential expression values significantly different (Benjamini-Hochberg-adjusted $p \leq 0.05$) between untreated and 100 nM BPA exposed samples. For all plots, the first in the series represents “Untreated” followed by “100 nM BPA exposed.” Note: BPA, bisphenol A; EpiLCs, epiblast-like cell; GO, gene ontology; RARE, retinoic acid response element; PGC, primordial germ cell; PGCLC, PGC-like cell.

Table 4. Calculated Wilcoxon paired sign rank test *p*-values of expression levels for different gene sets in PGCLCs derived from BPA-exposed EpiLCs.

| Gene set | Wilcoxon paired-sign rank test <i>p</i> -value | Median (log ₁₀) | | |
|--|--|-----------------------------|-----------|--------|
| | | No. genes analyzed | Untreated | 100 nM |
| Mouse conserved RARE | 0.0022 | 130 | 1.625 | 1.719 |
| GO:0042573: retinoic acid metabolic process | 0.0105 | 10 | 0.856 | 0.973 |
| GO:0042572: retinol metabolic processes | 0.0419 | 14 | 0.958 | 1.098 |
| GO:0051321: meiotic cell cycle | 0.0031 | 110 | 1.64 | 1.40 |
| GO:1901993: regulation of meiotic cell cycle phase transition | 0.0156 | 7 | 1.646 | 1.571 |
| GO:0070192: chromosome organization involved in meiotic cell cycle | 0.0391 | 8 | 2.041 | 1.934 |
| GO:0098762: meiotic cell cycle phase | 0.0273 | 9 | 1.612 | 1.608 |

Note: Data refers to Figure 5. BPA, bisphenol A; EpiLC, epiblast-like cell; PGC, primordial germ cell; PGCLC, PGC-like cell.

The continued enhanced proliferation observed in PGCLCs derived from BPA-exposed EpiLCs prompted us to examine whether there were any differences in expression levels of different factors listed in GO biological process terms associated with epigenetic processes. This examination revealed up-regulation of genes in two terms: GO: 000012 (negative regulation of transcription by RNA polymerase II) (Figure S12A) and GO: 1903319 (positive regulation of protein maturation) (Figure S12B). Interestingly, genes in GO terms associated with proteins involved in DNA methylation (GO: 0003606), histone methylation (GO: 0016571), and piRNA metabolic process (GO: 0034587) (Figure S12C–E) did not show significant

differences in expression between control and treated germ cells.

Analysis of Repeat Expression in PGCLCs Derived from BPA-Exposed EpiLCs

We examined whether there were any perturbations in repeat expression in untreated and exposed germ cells. We analyzed read counts mapping to all annotated mouse repeats listed on RepeatMasker (<http://repeatmasker.org>), focusing on those repeats that showed differential expression in untreated in comparison with exposed germ cells. This analysis revealed that

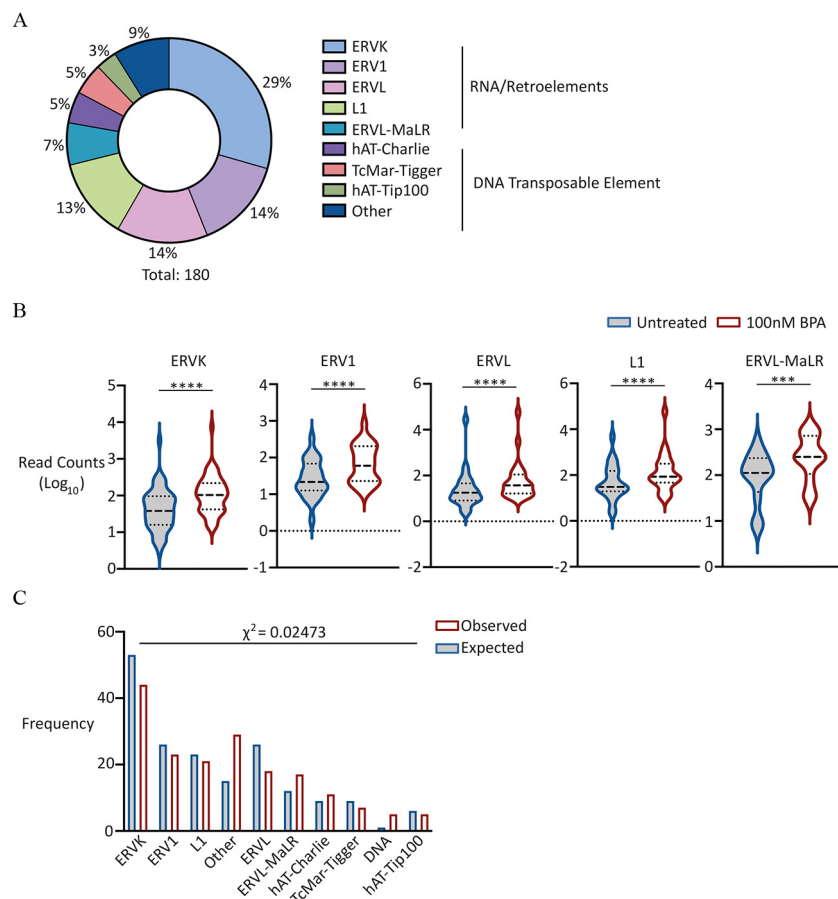


Figure 6. Analysis of repeat DNA expression in PGCLCs derived from EpiLCs exposed to 100 nM BPA. (A) Pie chart showing percentage distribution of different repeat families up-regulated in exposed germ cells. For full list of repeat families, see Excel Table S22. (B) Violin plots showing aggregate expression levels of different repeat families indicated, up-regulated in exposed germ cells. Dashed lines represent median and quartiles. Wilcoxon matched-pairs signed rank test *p*-values: <0.0001 (ERVK, ERV1, ERVL and L1); <0.001 for ERVL-MaR. First plot represents “Untreated” followed by “100 nM exposed.” (C) Bar graph comparing observed with expected frequency of different repeat families indicated, up-regulated in exposed germ cells. Expected frequencies of each family calculated based on total number of up-regulated repeat families and proportion occurrence in RepeatMasker database. First plot represents “Observed,” followed by “Expected” frequency. For the full list of up-regulated elements and repeat superfamilies, see Excel Tables S23 and S24, respectively. Note: BPA, bisphenol A; EpiLCs, epiblast-like cell; PGC, primordial germ cell; PGCLC, PGC-like cell.

although 10 repeat elements were down-regulated in PGCLCs derived from BPA-exposed EpiLCs (Excel Table S22), the vast majority (180 repeat elements) were up-regulated (Figure 6A,B; Excel Table S23, S24). More than three-quarters of the up-regulated elements belonged to five groups: ERVK, ERV1, ERVL, L1, and ERVL-MaLR. Using the proportion of all different repeat groups annotated in RepeatMasker, chi-square analysis was performed to determine if any groups displayed over- or underrepresentation (Figure 6C). This analysis revealed that aside from ERVL-MaLR, there was overrepresentation of ERVK, ERV1, ERVL, and L1 group elements ($\chi^2 = 0.025$). Because these groups contain young and presumably active retrotransposons, this finding supports the notion that these elements might therefore be coordinately regulated and therefore transcribed. However, our analysis of the RNA-seq data did not reveal significant differences in transcript levels of well-known restriction factors (Figure S13).

Discussion

Although a large body of animal-based studies exists on the reproductive impacts of BPA, to the best of our knowledge the data presented in this study are the first to reveal the specific impact of BPA-exposure in a model of the earliest stages of mammalian germ cell development. We found that EpiLCs displayed greater sensitivity toward BPA-exposure compared with ESCs, with exposed cells showing higher proliferation, lower apoptosis, and a higher proportion of cells staining positive for γ H2AX, a well-established marker of DNA damage. This higher proliferation had consequences on PGCLC formation, resulting in a higher number of PGCLCs formed in day 5 germ cell aggregates. Although expression analysis of known germ cell markers clearly showed that these cells retained a germ cell identity, they harbored altered expression of genes involved in ion and lipid transport, lipoprotein and steroid metabolism, and elevated retrotransposon expression. We were surprised to find that this behavior was not observed in a different cell line (BVSC-R8). Because BVSC-H18 is genetically female (XX), a possible explanation for this difference is the existence of sex-specific differences in the cell lines analyzed and their responsiveness to BPA. Female PGCLCs showed lower expression of X-linked genes, indicating that BPA exposure affected normal dosage compensation. Our results therefore provide evidence for the sensitivity of the PGC differentiation program and homeostasis to environmentally relevant levels of BPA.

BPA exposure of EpiLCs for a period of 24 h was sufficient to result in a higher number of cells recovered, in a concentration-dependent manner (Figure 1B). Intracellular staining followed by FACS indicated that this was correlated with a higher proportion of cells in S-phase as well as a lower proportion of apoptotic cells (Figure 1C–I). Collectively, these results show that the higher number of cells recovered following BPA exposure was in part a result of higher cell proliferation and lower apoptosis, despite signs of DNA damage in a higher proportion of cells. The effect on cell numbers in vertebrates is not unprecedented: A study in zebrafish involving BPA exposure of male embryos for 24 h post fertilization, during which time PGCs migrate and colonize the gonadal ridge, revealed that although exposure resulted in a reduction in the number of PGCs, there was no consequence on final testes development or fertility in the adult (Lombo et al. 2019), suggesting that BPA exposure results in “hyperproliferation” of the fewer founding PGCs and/or derivative cells as a compensatory mechanism in the future gonad.

Unsupervised differential gene expression analysis did not uncover significant transcriptional differences between control and BPA-exposed EpiLCs; this lack of significant difference might be attributed to the fact that cells were exposed for only 24 h, resulting

in insufficient time to detect widespread differences in gene expression. However, our targeted analysis of genes associated with DNA damage indicated higher expression of genes involved in DNA damage checkpoint control, specifically expression of factors involved in detecting the presence of DNA damage. Although γ H2AX is a molecular marker of DNA damage (Rogakou et al. 1998), it is also prevalent in highly proliferative cells, such as ES cells. In addition to this, it has been proposed that the presence of γ H2AX in ES cells is a consequence of global chromatin decondensation (Banáth et al. 2009). Although we cannot exclude the possibility that BPA exposure results in a further increase in chromatin decondensation, the fact that our data clearly showed higher proliferation as well higher expression of genes associated with DNA damage checkpoint control supports the notion that BPA is responsible for an elevation in DNA damage; the exact mechanisms, whether direct, indirect or both, remain to be determined.

The molecular underpinning responsible for enhanced proliferation remains unclear. Transcriptome analysis of untreated or 100 nM BPA-exposed EpiLCs did not reveal significant differences in gene expression (Excel Table S12). Despite this finding, there was evidence suggestive of epigenetic consequences on day 5 PGCLCs (DP). Although no longer exposed, these cells also showed higher proliferation (Figure 2B,G). We note that because nonPGCLCs (DN) and presumed transitioning cells (SP) also showed higher proliferation, this proliferation is likely a general effect on EpiLCs and resultant cell types, rather than a consequence specific to PGCLCs. An intriguing observation was the higher proportion of cells showing signs of DNA damage (Figure 1F–H). Previous data from a testicular coculture model indicated that BPA had no effect on the proportion of cells with signs of DNA damage when cultured for up to 72 h and at BPA concentrations up to 100 μ M (Yin et al. 2020). Consistent with this, 1-wk exposure of spermatogonial stem cell (SSC) cultures to 10 μ M BPA followed by testicular transplantation did not result in significant alterations in the presence of double-strand breaks in pachytene spermatocytes (Karmakar et al. 2017). Our results highlight differences in sensitivity based on developmental stage when exposure arises and suggests this aspect deserves greater attention when considering chemical toxicity on basic cell biological processes. Of particular concern, the presence of more cells with DNA damage has implications for the transmission of genetic lesions/mutations into later stages of germ cell development, which could have consequences for disease or the overall fitness of any resultant offspring.

The observation that BPA exposure had no discernible effect on PGCLCs derived from BVSC-R8 EpiLCs was unexpected but, in retrospect, perhaps not as surprising as it initially seems. Although we cannot rule out clonal differences between the BVSC-R8 and BVSC-H18 cell lines, we note that a key difference between these two cell lines is sex. Sex-specific gene expression differences in early embryonic cells, including ESCs and EpiLCs, have previously been reported (Lowe et al. 2015; Shirane et al. 2016), which presumably could affect responsiveness to BPA exposure. This hypothesis is supported by our finding that BPA exposure led to a significant deregulation of X-linked transcripts. In mammals, dosage of X-linked genes is regulated by X inactivation (Brockdorff et al. 1991), whereby expression of *Xist* coats and inactivates one of the two X chromosomes. Both X chromosomes are reportedly active in female EpiLCs (Hayashi et al. 2012) and in day 6 PGCLCs (Shirane et al. 2016). In light of this, our observation that PGCLCs derived from BPA-exposed BVSC-H18/female EpiLCs showed a disproportionate impact on X-linked genes suggests a disturbance in correct dosage regulation of genes located on the X chromosome and warrants further investigation. Taken together with our results, these observations suggest the existence of

sex-specific differences in the response of early germ cells to environmental exposures, prior to commitment to sexual fate.

Gene ontology analysis of transcriptome data from d5 PGCLCs derived from BPA-exposed EpiLCs indicated the enrichment of biological processes involved in lipid transport, lipoprotein metabolism and steroid metabolism (Figure 4; Excel Tables S16, S17). Our previous studies in *C. elegans* revealed a novel mechanism by which BPA interferes with steroidogenic acute regulatory (StAR) protein mediated cholesterol transport, resulting in reduced fertility (Chen et al. 2019). Up-regulation of genes involved in cholesterol biosynthesis supports the notion of a cholesterol imbalance in developing PGCLCs that might affect their normal function. In addition, the fact that pathways involved in cholesterol metabolism are also perturbed in this murine system underscores the high conservation of the pathways/processes affected by BPA in nematodes and mammals.

PGCs represent the immediate precursor stage before sexual differentiation. In the case of male gametogenesis, cells enter mitotic arrest and differentiate into prospermatogonia/gonocytes, whereas in females, cells enter meiosis I. Because PGCLCs derived from BPA-exposed EpiLCs exhibited transcriptional differences, we used a candidate approach to examine whether there were any effects on the expression levels of genes involved in later stages of gametogenesis (Figure 5). The mechanism by which meiosis is initiated depends on retinoic acid signaling, which induces, among other factors, *Stra8* expression (Baltus et al. 2006; Bowles et al. 2006). Our analyses suggest that although we did not find evidence of precocious meiotic entry, BPA exposure nonetheless resulted in transcriptional perturbations in GO categories implicated in RA signaling and meiotic regulation. Our inability to corroborate previous work suggesting a specific effect on RA signaling could be explained by methodological reasons. In contrast to our use of a defined protocol to specifically derive murine germ cells in the form of PGCLCs, Aoki and Takada investigated the effect of BPA exposure on embryoid bodies, which results in the formation of cells derived from all three germ layers (Aoki and Takada 2012).

Our transcriptomics analysis in PGCLCs does not unambiguously support a mechanism by which BPA may be acting on EpiLCs (i.e., binding to/activation of specific NHRs/pathways), and the effects on hormone signaling could be indirect and involve multiple pathways. Interestingly, our finding that *Hnf4a* transcript levels were higher recapitulates a previous study that showed that this gene is similarly perturbed by BPA in several tissues (Shu et al. 2019), suggesting this gene may be a general target deregulated by BPA, irrespective of cell type. Owing to the perturbations we detected in gene expression, our results suggest that BPA exposure may result in the formation of germ cells that are compromised in their function. For example, expression of *alpha-fetoprotein (Afp)* is substantially elevated in PGCLCs derived from BPA-exposed EpiLCs (Figure 3E; Excel Table S15). Through its capacity to bind estrogens at high affinity and thereby compete with cognate receptors (Uriel et al. 1976; Savu et al. 1981; Nishi et al. 1991) *Afp* is proposed to have antiestrogenic effects. Assuming this translates to protein expression, BPA-induced higher *Afp* expression level is therefore likely to have a negative rather than positive impact on estrogen signaling in PGCLCs. *In utero* exposure of mice to BPA during the formation of primary follicles has demonstrated an impact on germ cell nest breakdown, crucial in determining the size of the primary follicle and future fertility (Wang et al. 2014). Because this process is triggered by a drop in estrogen-mediated signaling, considering our data, it will be interesting to determine whether estrogen signaling is affected in PGCLCs derived from BPA-exposed EpiLCs that are subsequently used to generate primary oocytes. A modification of the PGCLC protocol has been successfully used to generate functional oocytes in culture (Hayashi et al. 2017), and the use of this expanded protocol in

future experiments could test the functional consequences of BPA-induced impacts on aspects of fertility such as primary follicle size.

A vital aspect of PGC differentiation is the need to silence repetitive elements, principally retrotransposons. The absence of mechanisms correctly regulating their expression has consequences on later fertility. For example, in E13.5 PGCs, endogenous retroviruses (ERVs) are repressed by the histone methyltransferase SET domain bifurcated histone lysine methyltransferase 1 (*Setdb1*), responsible for trimethylation of lysine position 9 of histone H3 (H3K9Me3) (Liu et al. 2014). Although germline conditional *Setdb1* mutant females do not show reduced numbers of PGCs, at postnatal day 10 (P10) these animals have smaller ovaries, with gonadal hypotrophy persisting through puberty and into adulthood (Liu et al. 2014). Our analysis of d5 PGCLC transcriptome data indicated that BPA exposure has an impact on retrotransposon regulation. We note that the libraries generated were enriched for polyadenylated mRNA. Given that the vast majority of repeats are not full-length but truncated and therefore lack a poly A tail (Lanciano and Cristofari 2020), it is likely that a large proportion of the repeat compartment, was under-represented in our data set. Correct repression of repeat elements, primarily RNA-based retrotransposons, is a crucial feature of normal germ cell development. Following global reductions in genome-wide levels of 5mC in CG contexts, and alterations in post-translational histone modifications (including H3K27me3 and H3K9me2/3) retrotransposons are activated; future studies examining the epigenome of PGCLCs derived from BPA-exposed EpiLCs should provide insight into whether repeat compartments harbor correct patterns of modifications and levels. Ordinarily, L1 elements are thought to be active between E13.5 to E16.5 in male and female germ cells (Seisenberger et al. 2012; Kobayashi et al. 2013). The higher expression of repeats induced by BPA is consistent with disruption in the normal mechanisms involved in their repression. Aside from histone methylation, the mammalian genome has evolved numerous host restriction mechanisms to control repeat expression at both the transcriptional and posttranscriptional levels (Goodier 2016). The nature of the mechanism(s) responsible for the elevation observed in repeat transcripts remains unclear. Although expression analysis of epigenetic factors and known host-encoded restriction factors are unchanged at the RNA level (Figure S13), it remains possible that prior exposure to BPA could alter protein levels, subcellular localization, and/or catalytic activity of one or more factors involved in regulating repeat expression. Recently in the context of epigenetic mechanisms, interest has centered on the importance of phase-separated condensates with liquidlike properties in the cell nucleus (reviewed by Bergeron-Sandoval et al. 2016). Germ cells, including PGCs, have such a structure termed “nuage,” which consists of (among other features) the chromatoid body (CB) (Kotaja and Sassone-Corsi 2007), itself enriched in repetitive RNA and RNA-binding proteins involved in repeat restriction such as *Ddx4/Mvh* (Meikar et al. 2014) and *Maelstrom* (Soper et al. 2008). Future experiments involving high-resolution imaging and using the PGCLC system could provide insight into whether the structure and/or composition of CB components is altered in cells derived from BPA-exposed EpiLCs. This approach could therefore provide a mechanism for the observed elevation of repeat transcripts.

In summary, to the best of our knowledge this study represents the first description of the consequences of toxicant exposure at a low, environmentally relevant concentration on the earliest stages of germ cell development. Together, our observations suggest that despite BPA-exposure increasing PGCLC formation, these cells are abnormal, and we posit that both their genetic and epigenetic content carry perturbations that are likely to affect the function of derivative gametes. Future studies will examine the nature of these consequences.

Acknowledgments

The authors want to thank A. Bline for help with BPA stock preparation. This work was supported by National Institute of Environmental Health Sciences R01 ES027487 and the John Templeton Foundation grant 60742.

The data generated for this study have been deposited in the Gene Expression Omnibus (<http://www.ncbi.nlm.nih.gov/geo/>) and are accessible through accession number GSE157570.

References

- Adler S, Pellizzer C, Paparella M, Hartung T, Bremer S. 2006. The effects of solvents on embryonic stem cell differentiation. *Toxicol In Vitro* 20(3):265–271, PMID: 16112835, <https://doi.org/10.1016/j.tiv.2005.06.043>.
- Allard P. 2014. Chapter 27: Bisphenol A. In: *Biomarkers in Toxicology*. Gupta RC, ed. Cambridge, MA: Academic Press, 459–474.
- Allard P, Colaiacovo MP. 2010. Bisphenol A impairs the double-strand break repair machinery in the germline and causes chromosome abnormalities. *Proc Natl Acad Sci USA* 107(47):20405–20410, PMID: 21059909, <https://doi.org/10.1073/pnas.1010386107>.
- Aoki T, Takada T. 2012. Bisphenol A modulates germ cell differentiation and retinoic acid signaling in mouse es cells. *Reprod Toxicol* 34(3):463–470, PMID: 22732146, <https://doi.org/10.1016/j.reprotox.2012.06.001>.
- Baltus AE, Menke DB, Hu YC, Goodheart ML, Carpenter AE, de Rooij DG, et al. 2006. In germ cells of mouse embryonic ovaries, the decision to enter meiosis precedes premeiotic DNA replication. *Nat Genet* 38(12):1430–1434, PMID: 17115059, <https://doi.org/10.1038/ng1919>.
- Ban ath JP, Ba uelos CA, Klovov D, MacPhail SM, Lansdorp PM, Olive PL, et al. 2009. Explanation for excessive DNA single-strand breaks and endogenous repair foci in pluripotent mouse embryonic stem cells. *Exp Cell Res* 315(8):1505–1520, PMID: 19154734, <https://doi.org/10.1016/j.yexcr.2008.12.007>.
- Barbonetti A, Castellini C, Di Giammarco N, Santilli G, Francavilla S, Francavilla F. 2016. In vitro exposure of human spermatozoa to bisphenol A induces pro-oxidative/apoptotic mitochondrial dysfunction. *Reprod Toxicol* 66:61–67, PMID: 27686954, <https://doi.org/10.1016/j.reprotox.2016.09.014>.
- Bergeron-Sandoval LP, Safaee N, Michnick SW. 2016. Mechanisms and consequences of macromolecular phase separation. *Cell* 165(5):1067–1079, PMID: 27203111, <https://doi.org/10.1016/j.cell.2016.05.026>.
- Bowles J, Knight D, Smith C, Wilhelm D, Richman J, Mamiya S, et al. 2006. Retinoid signaling determines germ cell fate in mice. *Science* 312(5773):596–600, PMID: 16574820, <https://doi.org/10.1126/science.1125691>.
- Brie no-Enr iquez MA, Robles P, Camats-Tarruella N, Garc a-Cruz R, Roig I, Cabero L, et al. 2011. Human meiotic progression and recombination are affected by bisphenol A exposure during in vitro human oocyte development. *Hum Reprod* 26(10):2807–2818, PMID: 21795248, <https://doi.org/10.1093/humrep/der249>.
- Brockdorff N, Ashworth A, Kay GF, Cooper P, Smith S, McCabe VM, et al. 1991. Conservation of position and exclusive expression of mouse Xist from the inactive X chromosome. *Nature* 351(6324):329–331, PMID: 2034279, <https://doi.org/10.1038/351329a0>.
- Chen Y, Panter B, Hussain A, Gibbs K, Ferreira D, Allard P. 2019. BPA interferes with StAR-mediated mitochondrial cholesterol transport to induce germline dysfunctions. *Reprod Toxicol* 90:24–32, PMID: 31445225, <https://doi.org/10.1016/j.reprotox.2019.08.001>.
- Chen J, Saili KS, Liu Y, Li L, Zhao Y, Jia Y, et al. 2017. Developmental bisphenol A exposure impairs sperm function and reproduction in zebrafish. *Chemosphere* 169:262–270, PMID: 27880925, <https://doi.org/10.1016/j.chemosphere.2016.11.089>.
- Dobin A, Davis CA, Schlesinger F, Drenkow J, Zaleski C, Jha S, et al. 2013. STAR: ultrafast universal RNA-seq aligner. *Bioinformatics* 29(1):15–21, PMID: 23104886, <https://doi.org/10.1093/bioinformatics/bts635>.
- Eden E, Navon R, Steinfeld I, Lipson D, Yakhini Z. 2009. Gorilla: a tool for discovery and visualization of enriched go terms in ranked gene lists. *BMC Bioinformatics* 10:48, PMID: 19192299, <https://doi.org/10.1186/1471-2105-10-48>.
- Garchon HJ, Loh E, Ho WY, Amar L, Avner P, Davis MM. 1989. The XLR sequence family: dispersion on the X and Y chromosomes of a large set of closely related sequences, most of which are pseudogenes. *Nucleic Acids Res* 17(23):9871–9888, PMID: 2602144, <https://doi.org/10.1093/nar/17.23.9871>.
- Gardner RL, Rossant J. 1979. Investigation of the fate of 4–5 day post-coitum mouse inner cell mass cells by blastocyst injection. *J Embryol Exp Morphol* 52:141–152, PMID: 521746.
- Ginsburg M, Snow MH, McLaren A. 1990. Primordial germ cells in the mouse embryo during gastrulation. *Development* 110(2):521–528, PMID: 2133553.
- Goodier JL. 2016. Restricting retrotransposons: a review. *Mob DNA* 7:16, PMID: 27525044, <https://doi.org/10.1186/s13100-016-0070-z>.
- Hales BF, Barton TS, Robaire B. 2005. Impact of paternal exposure to chemotherapy on offspring in the rat. *J Natl Cancer Inst Monogr* (34):28–31, PMID: 15784818, <https://doi.org/10.1093/jncimonographs/igi028>.
- Harkonen K. 2005. Pesticides and the induction of aneuploidy in human sperm. *Cytogenet Genome Res* 111:378–383, PMID: 16192720, <https://doi.org/10.1159/000086915>.
- Hassold T, Hunt P. 2001. To err (meiotically) is human: the genesis of human aneuploidy. *Nat Rev Genet* 2(4):280–291, PMID: 11283700, <https://doi.org/10.1038/35066065>.
- Hassold T, Hunt PA, Sherman S. 1993. Trisomy in humans: incidence, origin and etiology. *Curr Opin Genet Dev* 3(3):398–403, PMID: 8353412, [https://doi.org/10.1016/0959-437x\(93\)90111-2](https://doi.org/10.1016/0959-437x(93)90111-2).
- Hayashi K, Hikabe O, Obata Y, Hirao Y. 2017. Reconstitution of mouse oogenesis in a dish from pluripotent stem cells. *Nat Protoc* 12(9):1733–1744, PMID: 28796232, <https://doi.org/10.1038/nprot.2017.070>.
- Hayashi K, Ogushi S, Kurimoto K, Shimamoto S, Ohta H, Saitou M. 2012. Offspring from oocytes derived from in vitro primordial germ cell-like cells in mice. *Science* 338(6109):971–975, PMID: 23042295, <https://doi.org/10.1126/science.1226889>.
- Hayashi K, Ohta H, Kurimoto K, Aramaki S, Saitou M. 2011. Reconstitution of the mouse germ cell specification pathway in culture by pluripotent stem cells. *Cell* 146(4):519–532, PMID: 21820164, <https://doi.org/10.1016/j.cell.2011.06.052>.
- Hunt PA, Hassold TJ. 2008. Human female meiosis: what makes a good egg go bad? *Trends Genet* 24(2):86–93, PMID: 18192063, <https://doi.org/10.1016/j.tig.2007.11.010>.
- Hunt PA, Koehler KE, Susiarjo M, Hodges CA, Ilagan A, Voigt RC, et al. 2003. Bisphenol A exposure causes meiotic aneuploidy in the female mouse. *Curr Biol* 13(7):546–553, PMID: 12676084, [https://doi.org/10.1016/s0960-9822\(03\)00189-1](https://doi.org/10.1016/s0960-9822(03)00189-1).
- Karmakar PC, Kang H-G, Kim Y-H, Jung S-E, Rahman MS, Lee H-S, et al. 2017. Bisphenol A affects on the functional properties and proteome of testicular germ cells and spermatogonial stem cells *in vitro* culture model. *Sci Rep* 7(1):11858–11871, PMID: 28928476, <https://doi.org/10.1038/s41598-017-12195-9>.
- Kim D, Paggi JM, Park C, Bennett C, Salzberg SL. 2019. Graph-based genome alignment and genotyping with HISAT2 and HISAT-genotype. *Nat Biotechnol* 37(8):907–915, PMID: 31375807, <https://doi.org/10.1038/s41587-019-0201-4>.
- Kobayashi H, Sakurai T, Miura F, Imai M, Mochiduki K, Yanagisawa E, et al. 2013. High-resolution DNA methylome analysis of primordial germ cells identifies gender-specific reprogramming in mice. *Genome Res* 23(4):616–627, PMID: 23410886, <https://doi.org/10.1101/gr.148023.112>.
- Kotaja N, Sassone-Corsi P. 2007. The chromatoid body: a germ-cell-specific RNA-processing center. *Nat Rev Mol Cell Biol* 8(1):85–90, PMID: 17183363, <https://doi.org/10.1038/nrm2081>.
- Kuznetsova I, Lugmayr A, Siira SJ, Rackham O, Filipovska A. 2019. CirGO: an alternative circular way of visualising gene ontology terms. *BMC Bioinformatics* 20(1):84, PMID: 30777018, <https://doi.org/10.1186/s12859-019-2671-2>.
- Lal ev e S, Anno YN, Chatagnon A, Samarut E, Poch O, Laudet V, et al. 2011. Genome-wide in silico identification of new conserved and functional retinoic acid receptor response elements (direct repeats separated by 5 bp). *J Biol Chem* 286(38):33322–33334, PMID: 21803772, <https://doi.org/10.1074/jbc.M111.263681>.
- Lanciano S, Cristofari G. 2020. Measuring and interpreting transposable element expression. *Nat Rev Genet* 21(12):721–736, PMID: 32576954, <https://doi.org/10.1038/s41576-020-0251-y>.
- Larose H, Shami AN, Abbott H, Manske G, Lei L, Hammoud SS. 2019. Gametogenesis: a journey from inception to conception. *Curr Top Dev Biol* 132:257–310, PMID: 30797511, <https://doi.org/10.1016/bs.ctdb.2018.12.006>.
- Lerat E, Fablet M, Modolo L, Lopez-Maestre H, Vieira C. 2017. TETools facilitates big data expression analysis of transposable elements and reveals an antagonism between their activity and that of piRNA genes. *Nucleic Acids Res* 45(4):e17, PMID: 28204592, <https://doi.org/10.1093/nar/gkw953>.
- Li H, Handsaker B, Wysoker A, Fennell T, Ruan J, Homer N, et al. 2009. The Sequence Alignment/Map format and SAMtools. *Bioinformatics* 25(16):2078–2079, PMID: 19505943, <https://doi.org/10.1093/bioinformatics/btp352>.
- Liu S, Brind’Amour J, Karimi MM, Shirane K, Bogutz A, Lefebvre L, et al. 2014. Setdb1 is required for germline development and silencing of h3K9me3-marked endogenous retroviruses in primordial germ cells. *Genes Dev* 28(18):2041–2055, PMID: 25228647, <https://doi.org/10.1101/gad.244848.114>.
- Lombo M, Getino-Alvarez L, Depince A, Labbe C, Herrera MP. 2019. Embryonic exposure to bisphenol A impairs primordial germ cell migration without jeopardizing male breeding capacity. *Biomolecules* 9:307–320, PMID: 31349731, <https://doi.org/10.3390/biom9080307>.
- Lowe R, Gemma C, Rakyant VK, Holland ML. 2015. Sexually dimorphic gene expression emerges with embryonic genome activation and is dynamic throughout development. *BMC Genomics* 16:295–307, PMID: 25888192, <https://doi.org/10.1186/s12864-015-1506-4>.
- Mailhes JB, Young D, Caldito G, London SN. 2000. Sensitivity of mouse oocytes to nicotine-induced perturbations during oocyte meiotic maturation and aneuploidy in vivo and in vitro. *Mol Hum Reprod* 6(3):232–237, PMID: 10694270, <https://doi.org/10.1093/molehr/6.3.232>.

- Matuszczak E, Komarowska MD, Debek W, Hermanowicz A. 2019. The impact of bisphenol A on fertility, reproductive system, and development: a review of the literature. *Int J Endocrinol* 2019:4068717, PMID: 31093279, <https://doi.org/10.1155/2019/4068717>.
- Matzuk MM, Lamb DJ. 2008. The biology of infertility: research advances and clinical challenges. *Nat Med* 14(11):1197–1213, PMID: 18989307, <https://doi.org/10.1038/nm.f.1895>.
- Meikar O, Vagin VV, Chalmel F, Söstar K, Lardenois A, Hammell M, et al. 2014. An atlas of chromatoid body components. *RNA* 20(4):483–495, PMID: 24554440, <https://doi.org/10.1261/rna.043729.113>.
- Molyneaux KA, Stallock J, Schaible K, Wylie C. 2001. Time-lapse analysis of living mouse germ cell migration. *Dev Biol* 240(2):488–498, PMID: 11784078, <https://doi.org/10.1006/dbio.2001.0436>.
- Nishi S, Matsue H, Yoshida H, Yamaoto R, Sakai M. 1991. Localization of the estrogen-binding site of alpha-fetoprotein in the chimeric human-rat proteins. *Proc Natl Acad Sci USA* 88(8):3102–3105, PMID: 1707533, <https://doi.org/10.1073/pnas.88.8.3102>.
- Ohinata Y, Sano M, Shigeta M, Yamanaka K, Saitou M. 2008. A comprehensive, non-invasive visualization of primordial germ cell development in mice by the Prdm1-mVenus and Dppa3-ECFP double transgenic reporter. *Reproduction* 136(4):503–514, PMID: 18583473, <https://doi.org/10.1530/REP-08-0053>.
- Oosterhuis JW, Looijenga LH. 2005. Testicular germ-cell tumours in a broader perspective. *Nat Rev Cancer* 5(3):210–222, PMID: 15738984, <https://doi.org/10.1038/nrc1568>.
- Pacchierotti F, Ranaldi R. 2006. Mechanisms and risk of chemically induced aneuploidy in mammalian germ cells. *Curr Pharm Des* 12(12):1489–1504, PMID: 16611130, <https://doi.org/10.2174/138161206776389859>.
- Plahuta M, Tisler T, Pintar A, Toman MJ. 2015. Adverse effects of bisphenol A on water louse (*Asellus aquaticus*). *Ecotoxicol Environ Saf* 117:81–88, PMID: 25841063, <https://doi.org/10.1016/j.ecoenv.2015.03.031>.
- Prins GS, Patisaul HB, Belcher SM, Vandenberg LN. 2019. Clarity-BPA academic laboratory studies identify consistent low-dose bisphenol A effects on multiple organ systems. *Basic Clin Pharmacol Toxicol* 125(suppl 3):14–31, PMID: 30207065, <https://doi.org/10.1111/bcpt.13125>.
- Robinson MD, McCarthy DJ, Smyth GK. 2010. EdgeR: a Bioconductor package for differential expression analysis of digital gene expression data. *Bioinformatics* 26(1):139–140, PMID: 19910308, <https://doi.org/10.1093/bioinformatics/btp616>.
- Robinson MD, Oshlack A. 2010. A scaling normalization method for differential expression analysis of RNA-seq data. *Genome Biol* 11(3):R25, PMID: 20196867, <https://doi.org/10.1186/gb-2010-11-3-r25>.
- Rogakou EP, Pilch DR, Orr AH, Ivanova VS, Bonner WM. 1998. DNA double-stranded breaks induce histone H2AX phosphorylation on serine 139. *J Biol Chem* 273(10):5858–5868, PMID: 9488723, <https://doi.org/10.1074/jbc.273.10.5858>.
- Sahu C, Charaya A, Singla S, Dwivedi DK, Jena G. 2020. Zinc deficient diet increases the toxicity of bisphenol A in rat testis. *J Biochem Mol Toxicol* 34(10):e22549, PMID: 32609952, <https://doi.org/10.1002/jbt.22549>.
- Savu L, Benassayag C, Vallette G, Christeff N, Nunez E. 1981. Mouse alpha 1-fetoprotein and albumin. A comparison of their binding properties with estrogen and fatty acid ligands. *J Biol Chem* 256(18):9414–9418, PMID: 6169710.
- Seisenberger S, Andrews S, Krueger F, Arand J, Walter J, Santos F, et al. 2012. The dynamics of genome-wide DNA methylation reprogramming in mouse primordial germ cells. *Mol Cell* 48(6):849–862, PMID: 23219530, <https://doi.org/10.1016/j.molcel.2012.11.001>.
- Shareef A, Angove MJ, Wells JD, Johnson BB. 2006. Aqueous solubilities of estrone, 17 β -estradiol, 17 α -ethynylestradiol, and bisphenol A. *J Chem Eng Data* 51(3):879–881, <https://doi.org/10.1021/je050318c>.
- Shi YQ, Zhuang XJ, Xu B, Hua J, Liao SY, Shi Q, et al. 2013. SYCP3-like X-linked 2 is expressed in meiotic germ cells and interacts with synaptonemal complex central element protein 2 and histone acetyltransferase TIP60. *Gene* 527(1):352–359, PMID: 23810942, <https://doi.org/10.1016/j.gene.2013.06.033>.
- Shirane K, Kurimoto K, Yabuta Y, Yamaji M, Satoh J, Ito S, et al. 2016. Global landscape and regulatory principles of DNA methylation reprogramming for germ cell specification by mouse pluripotent stem cells. *Dev Cell* 39(1):87–103, PMID: 27642137, <https://doi.org/10.1016/j.devcel.2016.08.008>.
- Shu L, Meng Q, Diamante G, Tsai B, Chen YW, Mikhail A, et al. 2019. Prenatal bisphenol A exposure in mice induces multitissue multiomics disruptions linking to cardiometabolic disorders. *Endocrinology* 160(2):409–429, PMID: 30566610, <https://doi.org/10.1210/en.2018-00817>.
- Snow MH. 1981. Autonomous development of parts isolated from primitive-streak-stage mouse embryos. Is development clonal? *J Embryol Exp Morphol* 65(suppl):269–287, PMID: 7334310.
- Soper SF, van der Heijden GW, Hardiman TC, Goodheart M, Martin SL, de Boer P, et al. 2008. Mouse maelstrom, a component of nuage, is essential for spermatogenesis and transposon repression in meiosis. *Dev Cell* 15(2):285–297, PMID: 18694567, <https://doi.org/10.1016/j.devcel.2008.05.015>.
- Supek F, Bošnjak M, Škunca N, Šmuc T. 2011. REVIGO summarizes and visualizes long lists of gene ontology terms. *PLoS One* 6(7):e21800, PMID: 21789182, <https://doi.org/10.1371/journal.pone.0021800>.
- Susiarjo M, Hassold TJ, Freeman E, Hunt PA. 2007. Bisphenol A exposure in utero disrupts early oogenesis in the mouse. *PLoS Genet* 3(1):e5, PMID: 17222059, <https://doi.org/10.1371/journal.pgen.0030005>.
- Tanrikut C, Feldman AS, Altemus M, Paduch DA, Schlegel PN. 2010. Adverse effect of paroxetine on sperm. *Fertil Steril* 94(3):1021–1026, PMID: 19515367, <https://doi.org/10.1016/j.fertnstert.2009.04.039>.
- Tempamy JC, Zhou JH, Hodgkin PD, Bryant VL. 2018. Superior properties of CellTrace Yellow™ as a division tracking dye for human and murine lymphocytes. *Immunol Cell Biol* 96(2):149–159, PMID: 29363164, <https://doi.org/10.1111/imcb.1020>.
- Uriel J, Bouillon D, Aussel C, Dupiers M. 1976. Alpha-fetoprotein: the major high-affinity estrogen binder in rat uterine cytosols. *Proc Natl Acad Sci USA* 73(5):1452–1456, PMID: 58416, <https://doi.org/10.1073/pnas.73.5.1452>.
- Vandenberg LN, Hauser R, Marcus M, Olea N, Welshons WV. 2007. Human exposure to bisphenol A (BPA). *Reprod Toxicol* 24(2):139–177, PMID: 17825522, <https://doi.org/10.1016/j.reprotox.2007.07.010>.
- Wang W, Hafner KS, Flaws JA. 2014. In utero bisphenol a exposure disrupts germ cell nest breakdown and reduces fertility with age in the mouse. *Toxicol Appl Pharmacol* 276(2):157–164, PMID: 24576723, <https://doi.org/10.1016/j.taap.2014.02.009>.
- Wu H, Zhang Y. 2014. Reversing DNA methylation: mechanisms, genomics, and biological functions. *Cell* 156(1–2):45–68, PMID: 24439369, <https://doi.org/10.1016/j.cell.2013.12.019>.
- Yin L, Siracusa JS, Measel E, Guan X, Edenfield C, Liang S, et al. 2020. High-content image-based single-cell phenotypic analysis for the testicular toxicity prediction induced by bisphenol A and its analogs bisphenol S, bisphenol AF, and tetrabromobisphenol A in a three-dimensional testicular cell co-culture model. *Toxicol Sci* 173(2):313–335, PMID: 31750923, <https://doi.org/10.1093/toxsci/kfz233>.